

Discovery of WINERED-HVS1: A metal-rich hyper-velocity star candidate ejected from the Galactic center

KOHEI HATTORI,^{1,2,3} DAISUKE TANIGUCHI,¹ TAKUJI TSUJIMOTO,¹ NORIYUKI MATSUNAGA,^{4,5} HIROAKI SAMESHIMA,⁶
SCARLET S. ELGUETA,^{7,8} AND SHOGO OTSUBO⁵

¹National Astronomical Observatory of Japan, 2-21-1 Osawa, Mitaka, Tokyo 181-8588, Japan

²The Institute of Statistical Mathematics, 10-3 Midoricho, Tachikawa, Tokyo 190-8562, Japan

³Department of Astronomy, University of Michigan, 1085 S. University Avenue, Ann Arbor, MI 48109, USA

⁴Department of Astronomy, Graduate School of Science, The University of Tokyo, 7-3-1 Hongo, Bunkyo-ku, Tokyo 113-0033, Japan

⁵Laboratory of Infrared High-resolution spectroscopy (LiH), Koyama Astronomical Observatory, Kyoto Sangyo University, Motoyama, Kamigamo, Kita-ku, Kyoto 603-8555, Japan

⁶Institute of Astronomy, Graduate School of Science, The University of Tokyo, 2-21-1 Osawa, Mitaka, Tokyo 181-0015, Japan

⁷Departamento de Física, Universidad de Santiago de Chile, Av. Victor Jara 3659, Santiago, Chile

⁸Millenium Nucleus ERIS, Instituto de Estudios Astrofísicos, Universidad Diego Portales, Av. Ejército Libertador 441, Santiago, Chile

ABSTRACT

We report the discovery of a metal-rich red giant star, WINERED-HVS1, which is a candidate for a hyper-velocity star (HVS). Its past trajectory suggests that this star may have been ejected by the Galactic supermassive black hole (SMBH; Sgr A*), with a modest ejection velocity of at least 500 km s⁻¹. Since WINERED-HVS1 is gravitationally bound to the Milky Way and is not necessarily young, it is not an unambiguous HVS candidate from a kinematic perspective, unlike the previously confirmed A-type main-sequence HVS known as S5-HVS1. Therefore, the chemical characterization of this star is essential for understanding its origin. Through a spectroscopic follow-up observation with Magellan/WINERED, we determined its metallicity [Fe/H] = -0.147^{+0.046}_{-0.045}, as well as the abundances for Na, Mg, Si, S, K, Ca, Ti, Cr, Ni, and Sr. The high metallicity value suggests that this star was ejected from the Galactic center and is unlikely to be a halo star with a radial orbit. The abundance pattern of this star—including the pattern of [α/Fe], [Mg/Fe], [Si/Mg], and [Ca/Mg]—is consistent with that of the nuclear star cluster surrounding the SMBH, further supporting our view. This discovery opens a new window to look through the Galactic center environment without the hindrance of dust extinction, by using the HVSs moving in the halo region where dust extinction is minimal.

Keywords: – Hypervelocity stars (776) – High velocity stars (736) – Supermassive black holes (1663)
– Stellar abundances (1577)

1. INTRODUCTION

1.1. *Environment near the supermassive black hole in the Milky Way*

The center of the Milky Way is home to a supermassive black hole (SMBH) known as Sgr A*, which has a mass of $\sim 4 \times 10^6 M_{\odot}$ (Ghez et al. 2003; Gillessen et al. 2017). Although the intense tidal forces from this SMBH hinder star formation in its immediate vicinity (Levin 2007), observations have revealed that it is surrounded by a group of stars referred to as the S-stars. These stars orbit within a radius of 0.04 pc and include young massive stars. If we look further out, both the SMBH and the S-stars are contained within a nuclear

star cluster (NSC) that has a half light radius of ~ 4 pc and a total mass of $2\text{--}4 \times 10^7 M_{\odot}$ (Neumayer et al. 2020). The origins of these stellar components in the Galactic center remain a subject of ongoing debate (e.g., Guillard et al. 2016; Akiba et al. 2024). Studying this region is particularly challenging due to high levels of interstellar dust toward the Galactic center¹ (Carr et al. 2000; Ramírez et al. 2000; Cunha et al. 2007; Davies et al. 2009; Pfuhl et al. 2011; Rich et al. 2017; Ryde et al.

¹ When the manuscript of this paper was nearly ready for submission, we became aware of a study by Nandakumar et al. (2025) presenting the first results on the detailed chemical abundances of NSC stars. To maintain the independence of our analysis, we have not incorporated their findings in this paper. However, we fully acknowledge their pioneering contribution to this field. In our forthcoming paper (Taniguchi et al. in prep), we will discuss the implications from Nandakumar et al. (2025) in some detail.

Email: khattori@ism.ac.jp

Corresponding author: Kohei Hattori

2025; Nandakumar et al. 2025). Motivated by these difficulties, here we explore an alternative approach to infer the Galactic center environment, by using stars ejected from the SMBH, known as hyper-velocity stars (HVSs).

1.2. *Hyper-velocity stars as a new window to see the Galactic center environment*

Hills (1988) predicted that when the SMBH disrupts a binary star system, it gravitationally captures one star (forming an S-star²), while ejecting the other star with an ejection velocity of $\sim 10^3$ km s⁻¹, which is called an HVS.³ If such an HVS exists, it would convey information on the chemical abundances of stars near the SMBH (Koposov et al. 2020). HVSs are currently moving in the halo region, where the dust extinction is negligible. Therefore, finding HVSs in the halo and characterizing their chemical abundances may provide an access to the detailed chemical properties of the Galactic center.

Brown et al. (2005) discovered an unbound star named HVS1, which is a B-type star traveling at the heliocentric distance of ~ 39 – 71 kpc in the halo with a velocity of 709 km s⁻¹. Its metallicity is $[\text{Fe}/\text{H}] \simeq 0$, consistent with the Galactic center environment. Given the large velocity and the solar metallicity of this star, it is probably an HVS ejected by the SMBH, although the heliocentric distance is too uncertain that it is difficult to unambiguously trace back the orbit to the Galactic center. Later, Koposov et al. (2020) discovered an unambiguous HVS dubbed S5-HVS1, which is an A-type main-sequence star moving at 9 kpc from the Sun with a velocity of 1755 km s⁻¹. Due to its proximity from the Sun, its orbit can be traced back to the Galactic center with a small uncertainty. S5-HVS1 is currently the only unambiguous HVS from the Galactic center. Although the metallicity is estimated to be $[\text{Fe}/\text{H}] \simeq 0.29$ (Koposov et al. 2020), its detailed chemical abundances are yet to be determined due to its high temperature.

The ejection rate of HVSs is estimated to be one per $\sim 10^4$ years (Zhang et al. 2013; Brown 2015; Marchetti et al. 2018; see also Verberne et al. 2024). If HVSs travel with a velocity of $\sim 10^3$ km s⁻¹, a simple calculation suggests that there are $\sim 10^4$ HVSs within 100 kpc from the Galactic center (see Section 4.5 of Brown 2015; see also Marchetti et al. 2018). Considering that the stellar halo contains $\sim 10^9$ stars (Deason et al. 2019), only one in 10^5 of stars in the halo region is an HVS. The rarity of HVSs means that we need to search for HVSs from a large catalog. Following the major data releases from Gaia, namely Gaia DR2, EDR3, and DR3 (Gaia Collaboration et al. 2016, 2018, 2021, 2023), many authors have attempted to find HVSs from Gaia’s large 6D position-

velocity catalog (Hattori et al. 2018a; Marchetti et al. 2019; Marchetti 2021; Marchetti et al. 2022; Li et al. 2021). None of their fast-moving stars are unambiguous HVSs. This is partly because the stellar halo is dominated by halo stars with nearly radial orbits (Belokurov et al. 2018; Helmi et al. 2018).

Although previous kinematical searches for HVSs in the Gaia catalog did not result in discoveries of unambiguous HVSs, we still have a hope to find HVSs. Since typical stars near the Galactic center are much more metal-rich than field halo stars, HVSs should stand out when viewed in the chemistry space. Recently, extremely low-resolution stellar spectra named Gaia XP spectra were published for 219 million stars as part of the Gaia DR3 (De Angeli et al. 2023; Montegriffo et al. 2023). By using the Gaia XP spectra, Hattori (2025) estimated the metallicity $[\text{M}/\text{H}]_{\text{XP}}$ and α -abundance $[\alpha/\text{M}]_{\text{XP}}$ for 48 million stars in the low dust extinction regions. In this paper, we combine the chemical data from Hattori (2025) and the position/velocity data from Gaia DR3 to hunt for HVSs ejected from the Galactic center. By using Magellan/WINERED, we conduct a follow-up observation for the most metal-rich candidate, WINERED-HVS1, and we conclude that it is the most promising HVS candidate based on its chemistry.

1.3. *Structure of this paper*

This paper is organized as follows. Section 2 describes our strategy. Section 3 describes the data. Section 4 describes our assumptions on the Solar position and velocity. In Section 5, we first kinematically select 74 HVS candidates. Then we select 22 metal-rich HVS candidates by additionally using their chemistry. A follow-up observation for the most metal-rich HVS candidate (WINERED-HVS1) with Magellan/WINERED is described in Section 6. In Section 7, we demonstrate that WINERED-HVS1 is the most promising HVS candidate. In Section 8, we summarize our paper.

2. STRATEGY TO FIND HVS CANDIDATES

The aim of this paper is to find candidates of bound or unbound HVSs that were ejected from the Galactic center. As HVSs are no longer located in the Galactic center region, finding candidates of HVSs in the Gaia catalog (or any given stellar catalog) requires us to have a reliable model of the stellar orbits in the past. To build such a model, we need to know (i) the Galactic potential; (ii) the Solar position/velocity with respect to the Galactic center; and (iii) the stellar position/velocity relative to the Sun. If we had the perfect knowledge on (i)–(iii), finding HVSs would be straightforward because we would just need to trace the orbit backward in time and to find stars that ‘penetrate’ through the Galactic center. In reality, however, we have a limited understanding of (i)–(iii) mentioned above. To handle these uncertainties, we strategically design our HVS search as described below.

² The formation process of S-stars is not fully understood, and there may be multiple channels to form these stars. Binary disruption is one of the possible mechanisms to form S-stars.

³ In this paper, we define HVSs as those stars ejected from the Galactic center, regardless of their velocities.

Table 1. Four methods to kinematically search for HVS candidates

(1)	(2)	(3)
Search method	Potential model	Assumed (R_0, V_\odot)
Method A (fiducial)	McMillan (2017)	Fix (R_0, V_\odot)
Method B	McMillan (2017)	Vary (R_0, V_\odot)
Method C	Portail et al. (2017)	Fix (R_0, V_\odot)
Method D	Portail et al. (2017)	Vary (R_0, V_\odot)

NOTE— (1) Names of the search methods. Method A is the fiducial method. (2) Assumed Galactic potential. The model in McMillan (2017) is axisymmetric. The model in Portail et al. (2017) is a potential with a rotating bar (with a constant pattern speed $\Omega_{\text{bar}} = 39 \text{ kpc km s}^{-1}$). (3) The assumptions on the Solar position and velocity. (See Section 4 for details.)

Regarding the uncertainty associated with (i), we use two widely-used Galactic potential models (see Table 1). The fiducial model is an axisymmetric model explored by McMillan (2017), and the secondary model is a potential with a rotating bar (Portail et al. 2017). By using these two potentials, we can search for HVS candidates that are robust against the specific choice of the adopted potential. Also, we integrate the stellar orbits backward in time for only 200 Myr, and search for candidates of HVSs that have passed near the Galactic center within the last 200 Myr. Due to this short integration time, we essentially search for unbound HVSs; bound, recently-ejected HVSs that have not experienced disk crossing after ejection; or bound HVSs whose last disk crossings after the ejection were close to the Galactic center. (We may miss bound HVSs whose last disk crossings were not close to the Galactic center.) Because our inference on the stellar orbits becomes less reliable if we adopt longer integration time, our choice of short integration time minimizes the mis-classification of non-HVSs as HVS candidates.⁴

Regarding the uncertainty associated with (ii), we try two assumptions on the Solar position and velocity, $(\mathbf{x}_\odot, \mathbf{v}_\odot)$ (see Table 1). For Methods A and C, we fix $(\mathbf{x}_\odot, \mathbf{v}_\odot)$; while for Methods B and D, we try different set of $(\mathbf{x}_\odot, \mathbf{v}_\odot)$ each time we compute the stellar orbits (see Section 4). This is the first time the uncertainties in $(\mathbf{x}_\odot, \mathbf{v}_\odot)$ are taken into account in finding HVSs.⁵ Our investigation allows us to check how our search of HVSs are sensitive to the assumptions on \mathbf{x}_\odot and \mathbf{v}_\odot .

Regarding the uncertainty associated with (iii), for each star, we draw $N_{\text{MC}} = 10^4$ Monte Carlo samples

⁴ We choose a short integration time of 200 Myr, which makes our work distinct from Marchetti et al. (2022), who integrated the orbits for as long as 1 Gyr to search for HVS candidates.

⁵ There has been an attempt to determine $(\mathbf{x}_\odot, \mathbf{v}_\odot)$ by using an HVS (Koposov et al. 2020) with a method explored by Hattori et al. (2018b).

of the stellar position and velocity that reflect the observational uncertainty (see Section 3.2). For each star, we construct N_{MC} orbits in the last 200 Myr, which are used to select candidates of HVSs.

3. STELLAR DATA

Here we describe the data set used in this paper. Our notations are summarized in Table 6.

3.1. Selection of data

We construct the catalog of metal-rich stars by using the position-velocity data in Gaia DR3 catalog (Gaia Collaboration et al. 2023), the photometric distance from StarHorse catalog (Anders et al. 2022), and the chemical abundance catalog from Hattori (2025).

First, from Gaia DR3 catalog, we select stars with `parallax_over_error` > 5, with valid `radial_velocity` (v_{los}), and with $v_{\text{tot}} > 200 \text{ km s}^{-1}$. Here, v_{tot} is the point-estimate of the total velocity in the Galactocentric rest frame, derived with assumptions in Section 4.1. The selection by v_{tot} is not stringent, and it is set to reduce the computational cost in finding HVS candidates. The lower limit on v_{tot} is set for excluding some disk stars and excluding halo stars with low velocity. In computing v_{tot} , we use the point-estimate of the heliocentric stellar distance ($d = 1/\varpi$).

Secondly, we cross-match the catalog with the StarHorse catalog to obtain photometric distance information. As described in Section 3.2, we will use the 5th and 95th percentile values from the probability distribution of the photometric distance for each star, which are denoted as `dist05` and `dist95`.

Finally, we cross-match the sample with the chemical abundance catalog (<https://zenodo.org/records/10902172>) in Hattori (2025). To reduce the contamination from halo stars, we select stars with $[M/H]_{\text{XP}} > -1$ and `bool_flag_cmd_good=True`. The remaining 6.6×10^6 stars will be analyzed.

3.2. Monte Carlo realizations of the observed quantities of the star

Here we describe how we generate Monte Carlo realizations of the stellar position/velocity that reflect the uncertainties in the observed quantities. In the following, we focus on the procedure for i th star in our catalog.

For i th star, we draw $N_{\text{MC}} = 10^4$ realizations of the observable vector $(\alpha, \delta, d, \mu_{\alpha^*}, \mu_\delta, v_{\text{los}})$ by taking into account the associated error distribution, in a similar manner as in Okuno & Hattori (2022) and Hattori et al. (2023). We denote the j th realization of the observable vector (for star i) as

$$\mathbf{q}_{ij} = (\alpha^{(ij)}, \delta^{(ij)}, d^{(ij)}, \mu_{\alpha^*}^{(ij)}, \mu_\delta^{(ij)}, v_{\text{los}}^{(ij)}). \quad (1)$$

We neglect the tiny observational uncertainty in the sky coordinate, and thus we set $(\alpha^{(ij)}, \delta^{(ij)})$ to the observed

values in Gaia DR3 catalog. We draw the heliocentric distance $d^{(ij)}$ from the uniform distribution between $\text{dist05} < d < \text{dist95}$, where dist05 and dist95 are taken from the **StarHorse** catalog.⁶ We draw the proper motion vector $(\mu_{\alpha^*}^{(ij)}, \mu_{\delta}^{(ij)})$ from the error distribution in Gaia DR3 catalog, by taking into account the correlation between the two proper motion components. We draw the line-of-sight velocity $v_{\text{los}}^{(ij)}$ from the error distribution in Gaia DR3 catalog. After these procedures, for each star i , we obtain $N_{\text{MC}} = 10^4$ sets of phase-space vector \mathbf{q}_{ij} . The same sets of \mathbf{q}_{ij} will be analyzed with the four Methods A–D in [Table 1](#).

4. THE POSITION AND VELOCITY OF THE SUN

We use a right-handed Cartesian coordinate where the Galactic plane is the (x, y) -plane and z is directed to the North Galactic Pole. The Sun is located at $\mathbf{x}_{\odot} = (x, y, z)_{\odot} = (-R_0, 0, z_0)$. Its velocity is $\mathbf{v}_{\odot} = (v_x, v_y, v_z)_{\odot} = (U_{\odot}, V_{\odot}, W_{\odot})$. We fix $(\mathbf{x}_{\odot}, \mathbf{v}_{\odot})$ in Methods A and C; we vary them in Methods B and D.

4.1. Fixed Solar position and velocity: Methods A/C

For Methods A and C (see [Table 1](#)), we fix the Solar position and velocity. We assume $z_0 = 0.0208$ kpc ([Bennett & Bovy 2019](#)) and $(U_{\odot}, W_{\odot}) = (11.1, 7.25)$ km s⁻¹ ([Schönrich et al. 2010](#)). Also, we fix $(R_0, V_{\odot}) = (8.277 \text{ kpc}, 251.5 \text{ km s}^{-1})$ ([GRAVITY Collaboration et al. 2022](#); [Reid & Brunthaler 2020](#)).

4.2. Varied Solar position and velocity: Methods B/D

For Methods B and D (see [Table 1](#)), we take into account the uncertainties in $(\mathbf{x}_{\odot}, \mathbf{v}_{\odot})$. We prepare $N_{\text{MC}} = 10^4$ combinations of $(\mathbf{x}_{\odot}^{(j)}, \mathbf{v}_{\odot}^{(j)})$, where $j = 1, \dots, N_{\text{MC}}$, in the following manner. We assume the same fixed values for $(z_0, U_{\odot}, W_{\odot})$ as before. For (R_0, V_{\odot}) , we use $N_{\text{MC}} = 10^4$ pairs of values, $\{(R_0^{(j)}, V_{\odot}^{(j)}) \mid j = 1, \dots, N_{\text{MC}}\}$, which are drawn from:

$$R_0^{(j)} \sim \mathcal{N}(8.277, 0.1) \text{ kpc}, \quad (2)$$

$$\Omega_{\text{SgrA}}^{(j)} \sim \mathcal{N}(-6.411, 0.008) \text{ mas yr}^{-1}, \quad (3)$$

$$V_{\odot}^{(j)} = k R_0^{(j)} (-\Omega_{\text{SgrA}}^{(j)}), \quad (4)$$

with $k = 4.74047 \text{ km s}^{-1} \text{ kpc}^{-1} (\text{mas yr}^{-1})^{-1}$. Here, $a \sim \mathcal{N}(m, s)$ denotes that a is drawn from a Gaussian distribution with mean m and standard deviation s . We assume the uncertainty in R_0 to be 0.1 kpc ([Bland-Hawthorn & Gerhard 2016](#)). We assume that the angular motion of Sgr A* in the Galactic longitude direction, $\Omega_{\text{SgrA}} = -6.411 \pm 0.008 \text{ mas yr}^{-1}$ ([Reid & Brunthaler 2020](#)), corresponds to the Solar reflex motion.

⁶ We have confirmed that the most important HVS candidate in this paper (WINERED-HVS1) was also identified with our fiducial method (Method A), even if we set the upper and lower limits on the distance based on the zero-point-corrected Gaia parallax and its uncertainty.

5. SEARCH FOR HVS CANDIDATES

5.1. Backward orbit integration

Here we describe how we judge whether i th star in our catalog has a non-trivial probability of having been ejected by the SMBH.

From [Section 3.2](#), we have the position-velocity data of i th star relative to the Sun, represented by N_{MC} Monte Carlo samples. For j th Monte Carlo sample, we have the 6D observable vector \mathbf{q}_{ij} defined in equation (1). We convert \mathbf{q}_{ij} to the Galactocentric Cartesian position and velocity vector $(\mathbf{x}_{ij}, \mathbf{v}_{ij})$, by using the assumed Solar position and velocity $(\mathbf{x}_{\odot}, \mathbf{v}_{\odot})$. Here, we use the fixed value of $(\mathbf{x}_{\odot}, \mathbf{v}_{\odot})$ in Methods A and C, while we use $(\mathbf{x}_{\odot}, \mathbf{v}_{\odot}) = (\mathbf{x}_{\odot}^{(j)}, \mathbf{v}_{\odot}^{(j)})$ in Methods B and D. Then, from the current-day position-velocity $(\mathbf{x}_{ij}, \mathbf{v}_{ij})$, we integrate the orbit backward in time for 200 Myr in the model potential of the Milky Way, as shown in [Table 1](#).

If j th orbit of i th star crosses the disk plane at $-200 \text{ Myr} < t < 0 \text{ Myr}$, we record the last disk-crossing time $t = -\tau$ ($0 \text{ Myr} < \tau < 200 \text{ Myr}$). We record the position $\mathbf{x}_{\text{ej}} = (x_{\text{ej}}, y_{\text{ej}}, 0)$ at $t = -\tau$ and its Galactocentric radius $r_{\text{ej}} = (x_{\text{ej}}^2 + y_{\text{ej}}^2)^{1/2}$. Also, we record the velocity $\mathbf{v}_{\text{ej}} = (v_{x,\text{ej}}, v_{y,\text{ej}}, v_{z,\text{ej}})$ at $t = -\tau$ and its magnitude $v_{\text{ej}} = (v_{x,\text{ej}}^2 + v_{y,\text{ej}}^2 + v_{z,\text{ej}}^2)^{1/2}$.

For brevity, we call the disk-crossing position \mathbf{x}_{ej} and velocity \mathbf{v}_{ej} as the *ejection* position and *ejection* velocity, respectively, although their interpretation depends on the actual nature of i th star:

- If the star is an unbound HVS or a bound, recently-ejected HVS (ejected in the last 200 Myr), $(-\tau, \mathbf{x}_{\text{ej}}, \mathbf{v}_{\text{ej}})$ in our analysis correspond to the ejection time, ejection position, and ejection velocity of the HVS, respectively. (This is why we put the subscript ‘ej’ in these quantities.) The HVS’s flight time since the ejection is τ .
- If the star is a bound HVS that has experienced one or more disk crossings after the ejection (e.g., bound HVSs ejected more than 200 Myr ago), $(-\tau, \mathbf{x}_{\text{ej}}, \mathbf{v}_{\text{ej}})$ indicates the orbital properties of the HVS at the *last* disk crossing. If we assume that the Galactic potential has been approximately static, then the disk-crossing velocity should have been nearly the same whenever the star crossed the disk plane near the Galactic center. Therefore, the value of v_{ej} can be interpreted as the ejection velocity when it was originally ejected from the SMBH. Since we only consider the stellar orbit in the last 200 Myr, τ is not the flight time since the ejection, but is a lower limit on the flight time.
- If the star is not an HVS but an ordinary Galactic star, $(-\tau, \mathbf{x}_{\text{ej}}, \mathbf{v}_{\text{ej}})$ are their properties at the last disk crossing.

Although we trace the stellar orbit only in the last 200 Myr, the quantities such as $(\tau, r_{\text{ej}}, v_{\text{ej}})$ are still use-

ful to find candidates of HVSSs, as we will describe in [Section 5.2](#). (We admit, however, that the subscript ‘ej’ in r_{ej} or \mathbf{x}_{ej} may be misleading for bound HVSSs ejected long time ago or non-HVSSs.)

5.2. *Kinematically-selected HVS candidates*

For each Method (A–D), we conduct the backward orbit integration and derive \mathbf{x}_{ej} and \mathbf{v}_{ej} . Then we consider a star as a ‘kinematically-selected HVS candidate’ if at least one of the following conditions are satisfied:

- (Condition 1) For star i , count the number of Monte Carlo orbits that satisfy $r_{\text{ej}} < 50$ pc and $v_{\text{ej}} > 500$ km s⁻¹. If more than 1% of Monte Carlo orbits satisfy these conditions, we regard star i as an HVS candidate.
- (Condition 2) For star i , count the number of Monte Carlo orbits that satisfy $r_{\text{ej}} < 200$ pc and $v_{\text{ej}} > 500$ km s⁻¹. If more than 25% of Monte Carlo orbits satisfy these conditions, we regard star i as an HVS candidate.

These conditions are not mutually exclusive, so a star may satisfy both (Condition 1) and (Condition 2). (The number of kinematically-selected HVS candidates will be described in [Section 5.3](#).)

5.2.1. *Justification for (Condition 1) and (Condition 2)*

The purpose of (Condition 1) and (Condition 2) is to ensure that genuine, recently-ejected HVSSs are not missed, including both unbound HVSSs and bound ones that have not yet crossed the Galactic disk plane since their ejection.⁷ For example, suppose that we are confident on the assumed gravitational potential model and the Solar position and velocity. In this case, the uncertainty in the stellar orbit arises mainly from the uncertainty in the current-day position and velocity of the star. Since we have prepared a large number of Monte Carlo orbits per star, we believe that at least a small fraction of the Monte Carlo orbits are close to the genuine orbit and have small r_{ej} . Therefore, (Condition 1) works well to select HVS candidates.

In contrast, suppose that we are not very confident on the assumed gravitational potential model or the Solar position and velocity. In this case, a genuine, recently-ejected HVS may not have very small r_{ej} if the assumed potential is not a good approximation to the actual Milky Way potential. In order to investigate how the wrongly-assumed potential models affect the value of r_{ej} , we conduct a simple test. Here, we eject HVSSs from the Galactic center (with ejection velocity of ~ 600 km s⁻¹

and flight time of ~ 30 Myr) assuming a realistic potential model (the model in [McMillan 2017](#)) and rewinding the orbit backward in time in another realistic potential (the model in [Portail et al. 2017](#)) until the disk crossing. In this test, we do not assign observational errors, because we are interested in the systematic uncertainty in the ejection position arising purely from the choice of the gravitational potential. As a result, we find that $r_{\text{ej}} < 200$ pc is satisfied for the majority ($\sim 80\%$) of simulated HVSSs. Our simplified test suggests that a genuine, recently-ejected HVS probably satisfy $r_{\text{ej}} < 200$ pc. Therefore, (Condition 2) works well to select HVS candidates.

5.3. *Number of kinematically-selected HVS candidates*

After searching for the kinematically-selected HVS candidates with Methods A–D, we compared the list of candidates for each method. It turned out that the kinematically-selected HVS candidates mainly depend on the assumed potential and only weakly depend on the Solar position and velocity. Given that the list of kinematically-selected HVS candidates depends on the assumed potential, it is reassuring to note that 74 stars are regarded as kinematically-selected HVS candidates for all the methods we explored. It turned out that all of these 74 candidates are bound to the Milky Way. In the following, we will analyze these 74 kinematically-selected HVS candidates in more detail.

5.4. *Further pruning of HVS candidates with chemistry*

From the 74 kinematically-selected HVS candidates, we further select 22 metal-rich HVS candidates as summarized in [Fig. 1](#).

First, we remove 4 RR Lyrae stars by using an RR Lyrae catalog [Clementini et al. \(2023\)](#) and SIMBAD. Among the remaining 70 stars, 10 stars have reliable chemistry from either APOGEE DR17 ([Abdurro’uf et al. 2022](#)), GALAH DR4 ([Buder et al. 2024](#)), RAVE DR6 ([Steinmetz et al. 2020](#)), LAMOST DR9 v2.0 ([Zhao et al. 2012](#)). Among these stars, 9 stars satisfy⁸ $[\text{Fe}/\text{H}]_{\text{spec}} > -1$. We refer to these stars as ‘spectroscopically confirmed metal-rich HVS candidates’ and label them as mrHVSspec1-9. All of them are red giants.

For the 60 stars without spectroscopic chemical abundances, we use the chemical abundances ($[\text{M}/\text{H}]_{\text{XP}}$, $[\alpha/\text{M}]_{\text{XP}}$) taken from [Hattori \(2025\)](#) (see [Table 6](#)). We select 13 stars that satisfy the quality criteria in [Hattori \(2025\)](#), while showing $[\text{M}/\text{H}]_{\text{XP}} > -1$.⁹ We refer to these stars as ‘XP-based metal-rich HVS candidates.’ We label the most metal-rich candidate as WINERED-

⁸ Throughout this paper, $[\text{X}/\text{Y}]_{\text{spec}}$ denotes the spectroscopic measurements of $[\text{X}/\text{H}]$. See [Table 6](#).

⁹ We have already applied the cut $[\text{M}/\text{H}]_{\text{XP}} > -1$ in [Section 3](#). We show this cut also in [Fig. 1](#) just to emphasize that XP-based metal-rich HVS candidates do not include metal-poor stars.

⁷ We designed (Condition 1) and (Condition 2) to search for HVSSs that have been recently ejected from the Galactic center. However, with these conditions, we may also detect bound HVSSs whose last disk crossings were close to the Galactic center region.

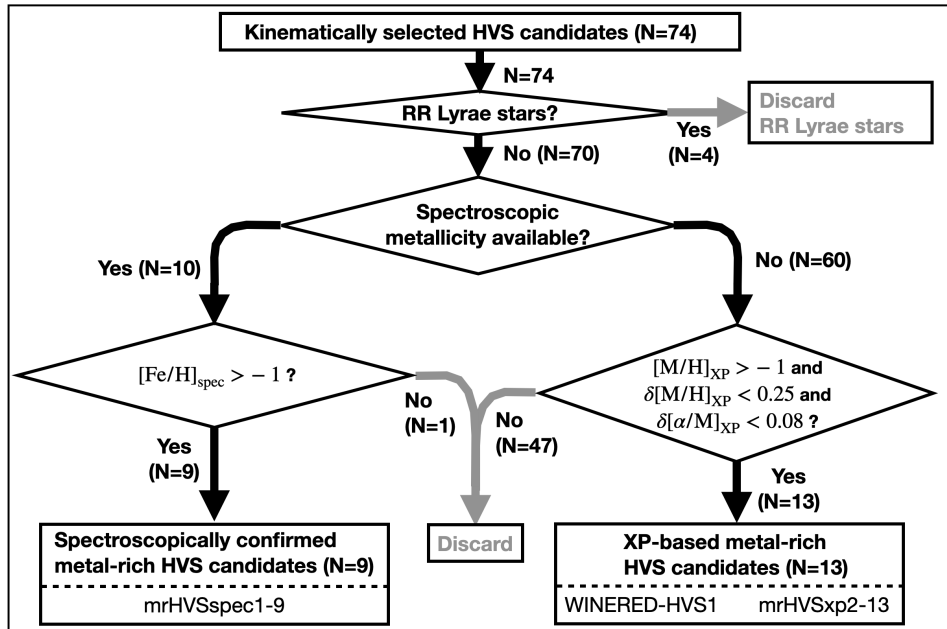


Figure 1. Flow chart to chemically select 22 metal-rich HVS candidates from the 74 kinematically selected HVS candidates. We refer to the 9 candidates with spectroscopic chemistry from literature as ‘spectroscopically confirmed metal-rich HVS candidates.’ We refer to the remaining 13 candidates as ‘XP-based metal-rich HVS candidates.’ The most metal-rich candidate, WINERED-HVS1, is among the XP-based metal-rich HVS candidates.

HVS1, while we label the rest of them as mrHVSxp2-13. Again, all of these candidates are red giants.

As can be inferred from the unique name convention for WINERED-HVS1, we regard this star different from other HVS candidates because it has intriguing chemical properties. Its XP-based metallicity, $[M/H]_{XP} = -0.23$, is higher than any other HVS candidates analyzed in this paper. Also, its α -abundance, $[\alpha/M]_{XP} = 0.06$, is one of the least α -enhanced stars in our HVS candidates. At face value, the metal-rich and α -poor nature of WINERED-HVS1 is reminiscent of the stellar population near the Galactic center region. We did a follow-up observation of this star with Magellan/WINERED and spectroscopically confirmed the metal-rich and α -poor nature of this star (see Section 6). Kinematics and chemistry of the 22 HVS candidates, including WINERED-HVS1, will be discussed in Section 7.

6. SPECTROSCOPIC OBSERVATION OF A HYPER-VELOCITY STAR CANDIDATE WINERED-HVS1

We obtained a near-infrared YJ -band high-resolution spectrum of WINERED-HVS1 using the WINERED spectrograph (0.90–1.35 μm with $R = 28,000$; Ikeda et al. 2022) attached to the Magellan Clay Telescope on June 6th 2023. We performed the ABBA nodding with 600sec exposures. With the J -band magnitude of 12.69 (2MASS; Cutri et al. 2003), the resultant signal-to-noise ratio (S/N) per pixel is 40–115 for the Y band (0.97–1.09 μm) and 25–90 for the J band (1.15–1.32 μm). We also observed a telluric-standard

A0V star, HD 170115, with a sufficient S/N of 200–400. The raw data was reduced using the WINERED Automatic Reduction Pipeline (WARP version 3.8.7; Hamano et al. 2024), and telluric lines were removed with the standard star using the method described by Sameshima et al. (2018). Then the line-of-sight velocity was determined using the cross-correlation function between the observed spectrum and a radial velocity template spectrum, and the wavelengths were adjusted to the standard-air scale at rest. The reduced spectrum, together with the best-fit synthetic spectrum whose parameters will be determined in this section, is shown in Figs. 2 and 3.

After thorough examination, we concluded that the systematic bias in the determined line-of-sight velocity, summarized in Table 4, would be $\sim 1.0 \text{ km s}^{-1}$ at most. Our line-of-sight velocity measurement for this star ($34.79 \pm 0.13(\text{rand.}) \pm 1.0(\text{sys.}) \text{ km s}^{-1}$) differs from the value reported in Gaia DR3 ($26.52 \pm 2.07 \text{ km s}^{-1}$). To maintain consistency across all stars in our sample, we adopt the Gaia DR3 line-of-sight velocity for this star in our orbital analysis. We have confirmed that adopting the value from our follow-up spectroscopic data has a minor effect on the orbital analysis for this star (e.g., reducing the value of v_{ej} by $\sim 25 \text{ km s}^{-1}$), which does not affect the main conclusion of this paper.

With the reduced spectrum, we determined chemical abundances of WINERED-HVS1 with a method similar to those performed by Kondo et al. (2019) and Fukue et al. (2021) using the OCTOMAN code (Taniguchi et al. 2025), which is a wrapper of the spectral synthesis code

Table 2. Kinematical properties of our HVS candidates

(1)	(2)	(3)	(4)	(5)	(6)	(7)	(8)	(9)	(10)	(11)
Name	DR3 source_id	$(f_{50 \text{ pc}}, f_{200 \text{ pc}})$	r_{ej}	v_{ej}	τ	(x, y, z)	(r, R)	(v_x, v_y, v_z)	(v_r, v_R, v_ϕ)	v
			pc	km s ⁻¹	Myr	kpc	kpc	km s ⁻¹	km s ⁻¹	km s ⁻¹
mrHVSspec1	1364083369852936576	[0.2525, 0.9708]	0	535	26	[-7.60, +2.69, +1.60]	[8.22, 8.06]	[-175, +62, -7]	[-181, +186, -0]	186
mrHVSspec2	3894254612584073472	[0.0218, 0.1212]	1	578	22	[-8.04, -1.21, +2.82]	[8.60, 8.13]	[-265, -40, +60]	[-273, +268, -0]	275
mrHVSspec3	6508950579775204864	[0.0359, 0.0943]	1	606	15	[-4.09, -1.67, -5.26]	[6.87, 4.42]	[-221, -90, -258]	[-351, +238, +0]	351
mrHVSspec4	2694242193191538816	[0.1053, 0.8001]	1	533	24	[-7.54, +1.29, -1.09]	[7.73, 7.65]	[-197, +34, +16]	[-196, +200, +0]	201
mrHVSspec5	6137389419947219584	[0.0000, 0.2973]	54	521	23	[-4.44, -5.08, +2.37]	[7.15, 6.75]	[-122, -136, +21]	[-180, +183, -3]	184
mrHVSspec6	5467370673479835904	[0.0001, 0.3035]	46	571	21	[-8.28, -1.63, +0.74]	[8.47, 8.44]	[-268, -55, -10]	[-272, +274, +2]	274
mrHVSspec7	6692069426721736832	[0.0504, 0.0536]	5	501	11	[-2.76, +0.21, -2.83]	[3.96, 2.77]	[-186, +14, -153]	[-239, +186, +1]	241
mrHVSspec8	3552388581761193728	[0.0339, 0.1519]	3	556	25	[-8.26, -2.33, +1.72]	[8.76, 8.59]	[-219, -62, +7]	[-224, +227, +0]	227
mrHVSspec9	3657091157063641344	[0.0120, 0.1198]	2	543	21	[-6.33, -1.04, +3.20]	[7.17, 6.42]	[-214, -35, +71]	[-226, +217, -0]	228
WINERED-HVS1	6434696676903108864	[0.0310, 0.4957]	16	537	14	[-4.44, -2.30, -2.18]	[5.45, 5.00]	[-232, -122, -76]	[-270, +262, +1]	273
mrHV Sxp2	4548672495942395264	[0.1131, 0.4637]	0	544	15	[-4.75, +2.81, +1.89]	[5.84, 5.52]	[-234, +138, +54]	[-274, +271, +0]	277
mrHV Sxp3	6173750574418020352	[0.0469, 0.0564]	1	502	25	[-3.60, -3.97, +3.69]	[6.51, 5.36]	[-83, -92, +40]	[-125, +124, -0]	130
mrHV Sxp4	4572287497444895104	[0.0914, 0.3728]	1	556	17	[-5.44, +2.72, +2.74]	[6.67, 6.09]	[-233, +117, +81]	[-271, +261, +0]	273
mrHV Sxp5	6307609625404677376	[0.0147, 0.1091]	7	540	13	[-2.82, -1.46, +4.01]	[5.12, 3.18]	[-164, -84, +200]	[-272, +185, -0]	272
mrHV Sxp6	5765626877690171904	[0.0034, 0.2743]	7	518	23	[-6.41, -2.59, -1.46]	[7.06, 6.91]	[-168, -68, +10]	[-175, +181, -0]	182
mrHV Sxp7	6773393846499438464	[0.0349, 0.1637]	3	503	77	[-2.73, +1.92, -1.81]	[3.80, 3.34]	[-120, -84, +223]	[-235, -146, -0]	267
mrHV Sxp8	6425246443181463680	[0.0188, 0.1082]	2	532	18	[-3.37, -3.02, -4.16]	[6.15, 4.53]	[-136, -122, -133]	[-225, +183, +0]	226
mrHV Sxp9	4501932497166815360	[0.0009, 0.2663]	30	547	18	[-1.69, +6.03, +2.79]	[6.85, 6.26]	[-64, +232, +71]	[-249, +241, -1]	251
mrHVSxp10	1497611497903517056	[0.0534, 0.5141]	2	568	23	[-8.08, +0.86, +2.45]	[8.48, 8.12]	[-253, +27, +41]	[-255, +254, +0]	257
mrHVSxp11	1329060763412103808	[0.0159, 0.3891]	8	579	19	[-6.42, +2.75, +3.42]	[7.78, 6.98]	[-251, +107, +101]	[-289, +273, +1]	291
mrHVSxp12	5130376441238310016	[0.0426, 0.2071]	0	575	33	[-10.16, -0.71, -4.35]	[11.07, 10.18]	[-205, -14, -57]	[-212, +206, +0]	214
mrHVSxp13	3929723865560075776	[0.0238, 0.1063]	2	598	25	[-7.28, -1.31, +6.65]	[9.95, 7.39]	[-220, -39, +177]	[-284, +223, -0]	285

NOTE— (1) Name of the metal-rich HVS candidates. Stars named mrHVSspec1-9 are HVS candidates for which we have spectroscopic abundance information from publicly available data. For WINERED-HVS1, we have spectroscopic abundance information from our follow-up observations with Magellan/WINERED. Stars named mrHVSxp2-15 are HVS candidates for which we have the abundance information from the Gaia XP spectra only. (2) Gaia DR3 source id. (3) The fraction of orbits that pass within the specified Galactocentric radius (50 pc and 200 pc) in the last 200 Myr with a large ejection velocity (disk-crossing velocity) of $v_{\text{ej}} > 500 \text{ km s}^{-1}$. (4)-(5) The ejection radius $r_{\text{ej}} = |\mathbf{x}_{\text{ej}}|$ and ejection velocity $v_{\text{ej}} = |\mathbf{v}_{\text{ej}}|$ in the best orbit. Here, the best orbit is chosen among $N_{\text{MC}} = 10001$ Monte Carlo orbits such that the ejection position is closest to the Galactic center while having a large ejection velocity ($v_{\text{ej}} > 500 \text{ km s}^{-1}$). (6) The time since the last disk crossing in the best orbit. If our candidates are recently-ejected HVSs, this quantity corresponds to the flight time since the ejection from the Galactic center. (7)-(8) The current Galactocentric spherical radius (r) and cylindrical radius (R) of the star in the best orbit, respectively. (9)-(11) The current velocity of the star in the best orbit. Here, $v = |\mathbf{v}|$ is the magnitude of the current velocity.

Table 3. Chemical properties of our HVS candidates

(1)	(2)	(3)	(4)	(5)	(6)	(7)	(8)	(9)	(10)	(11)
Name	DR3 source_id	[Fe/H] _{spec} dex	[Mg/Fe] _{spec} dex	[Si/Fe] _{spec} dex	[Ca/Fe] _{spec} dex	[Ti/Fe] _{spec} dex	[Al/Fe] _{spec} dex	[α/Fe] _{spec} dex	[M/H] _{XP} dex	[α/M] _{XP}
mrHVSspec1	1364083369852936576	-0.64 ± 0.01	0.35 ± 0.01	0.23 ± 0.02	0.18 ± 0.02	0.12 ± 0.02	0.27 ± 0.02	0.22 ± 0.09	-0.64 ^{+0.18} _{-0.00}	+0.29 ^{+0.00} _{-0.05}
mrHVSspec2	3894254612584073472	-0.81 ± 0.01	0.18 ± 0.02	0.08 ± 0.03	0.18 ± 0.03	0.12 ± 0.04	-0.25 ± 0.03	0.14 ± 0.04	-0.83 ^{+0.14} _{-0.17}	+0.26 ^{+0.05} _{-0.00}
mrHVSspec3	6508950579775204864	-0.50 ± 0.06	0.22 ± 0.02	0.34 ± 0.02	-0.09 ± 0.02	0.02 ± 0.01	-0.43 ± 0.02	0.12 ± 0.17	-0.86 ^{+0.07} _{-0.17}	+0.11 ^{+0.05} _{-0.07}
mrHVSspec4	2694242193191538816	-0.66 ± 0.06	0.39 ± 0.04	0.29 ± 0.03	0.40 ± 0.04	0.28 ± 0.06	0.13 ± 0.11	0.34 ± 0.06	-0.77 ^{+0.27} _{-0.10}	+0.28 ^{+0.03} _{-0.05}
mrHVSspec5	6137389419947219584	-0.83 ± 0.06	0.32 ± 0.03	0.32 ± 0.02	0.24 ± 0.04	0.21 ± 0.02	0.09 ± 0.04	0.27 ± 0.05	-0.97 ^{+0.16} _{-0.13}	+0.07 ^{+0.05} _{-0.04}
mrHVSspec6	5467370673479835904	-0.98 ± 0.07	0.10 ± 0.07	0.30 ± 0.05	0.34 ± 0.06	0.72 ± 0.17	-	0.37 ± 0.22	-1.00 ^{+0.44} _{-0.44}	+0.15 ^{+0.20} _{-0.11}
mrHVSspec7	6692069426721736832	-0.47 ± 0.13	-	-	-	-	0.14 ± 0.13	0.52 ± 0.18	-0.64 ^{+0.10} _{-0.10}	+0.31 ^{+0.04} _{-0.07}
mrHVSspec8	3552388581761193728	-0.90 ± 0.13	-	-	-	-	0.23 ± 0.13	0.39 ± 0.25	-0.95 ^{+0.17} _{-0.16}	+0.22 ^{+0.07} _{-0.08}
mrHVSspec9	3657091157063641344	-0.39	-	-	-	-	-	-	-0.45 ^{+0.09} _{-0.12}	+0.25 ^{+0.05} _{-0.05}
WINERED-HVS1	6434696676903108864	-0.147 ^{+0.046} _{-0.045}	-0.058 ^{+0.077} _{-0.082}	0.144 ^{+0.088} _{-0.091}	-0.001 ^{+0.175} _{-0.177}	0.008 ^{+0.140} _{-0.151}	-	0.02 ± 0.07	-0.23 ^{+0.08} _{-0.08}	+0.06 ^{+0.04} _{-0.02}
mrHVSxp2	4548672495942395264	-	-	-	-	-	-	-	-0.40 ^{+0.11} _{-0.11}	+0.25 ^{+0.04} _{-0.03}
mrHVSxp3	6173750574418020352	-	-	-	-	-	-	-	-0.56 ^{+0.10} _{-0.12}	+0.15 ^{+0.04} _{-0.04}
mrHVSxp4	4572287497444895104	-	-	-	-	-	-	-	-0.59 ^{+0.10} _{-0.16}	+0.27 ^{+0.02} _{-0.06}
mrHVSxp5	6307609625404677376	-	-	-	-	-	-	-	-0.63 ^{+0.16} _{-0.15}	+0.26 ^{+0.04} _{-0.07}
mrHVSxp6	5765626877690171904	-	-	-	-	-	-	-	-0.69 ^{+0.19} _{-0.22}	+0.25 ^{+0.05} _{-0.07}
mrHVSxp7	6773393846499438464	-	-	-	-	-	-	-	-0.71 ^{+0.14} _{-0.14}	+0.28 ^{+0.05} _{-0.04}
mrHVSxp8	6425246443181463680	-	-	-	-	-	-	-	-0.73 ^{+0.17} _{-0.17}	+0.27 ^{+0.04} _{-0.08}
mrHVSxp9	4501932497166815360	-	-	-	-	-	-	-	-0.84 ^{+0.18} _{-0.25}	+0.07 ^{+0.08} _{-0.03}
mrHVSxp10	1497611497903517056	-	-	-	-	-	-	-	-0.85 ^{+0.11} _{-0.12}	+0.28 ^{+0.04} _{-0.04}
mrHVSxp11	1329060763412103808	-	-	-	-	-	-	-	-0.91 ^{+0.19} _{-0.27}	+0.25 ^{+0.05} _{-0.07}
mrHVSxp12	5130376441238310016	-	-	-	-	-	-	-	-0.93 ^{+0.17} _{-0.17}	+0.27 ^{+0.07} _{-0.07}
mrHVSxp13	3929723865560075776	-	-	-	-	-	-	-	-0.96 ^{+0.16} _{-0.15}	+0.17 ^{+0.07} _{-0.06}

NOTE—(1) Name of the metal-rich HVS candidates. (2) Gaia DR3 source id. (3)-(9) Chemical abundances from spectroscopic observations. The spectroscopic data for mrHVSspec1-2 are taken from APOGEE DR17 (Aburro et al. 2022), those for mrHVSspec3-6 are taken from GALAH DR4 (Buder et al. 2024), those for mrHVSspec7-8 are taken from RAVE DR6 (Steinmetz et al. 2020), those for mrHVSspec9 are taken from LAMOST DR9 v2.0 (Zhao et al. 2012), and those for WINERED-HVS1 are derived from our analysis in Section 6. (We note that mrHVSspec4 is flagged as a single-line spectroscopic binary in GALAH data.) For mrHVSxp1-6, we adopt $[\alpha/\text{Fe}]_{\text{spec}} = ([\text{Mg}/\text{Fe}]_{\text{spec}} + [\text{Si}/\text{Fe}]_{\text{spec}} + [\text{Ca}/\text{Fe}]_{\text{spec}} + [\text{Ti}/\text{Fe}]_{\text{spec}})/4$ (see also Table 6 for the definition of $[\alpha/\text{Fe}]_{\text{spec}}$). For mrHVSxp7-8, we adopt $[\alpha/\text{Fe}]_{\text{spec}}$ from RAVE DR6. (10)-(11) The metallicity $[\text{M}/\text{H}]_{\text{XP}}$ and α -abundance $[\alpha/\text{M}]_{\text{XP}}$ estimated from Gaia XP spectra (Hattori 2025).

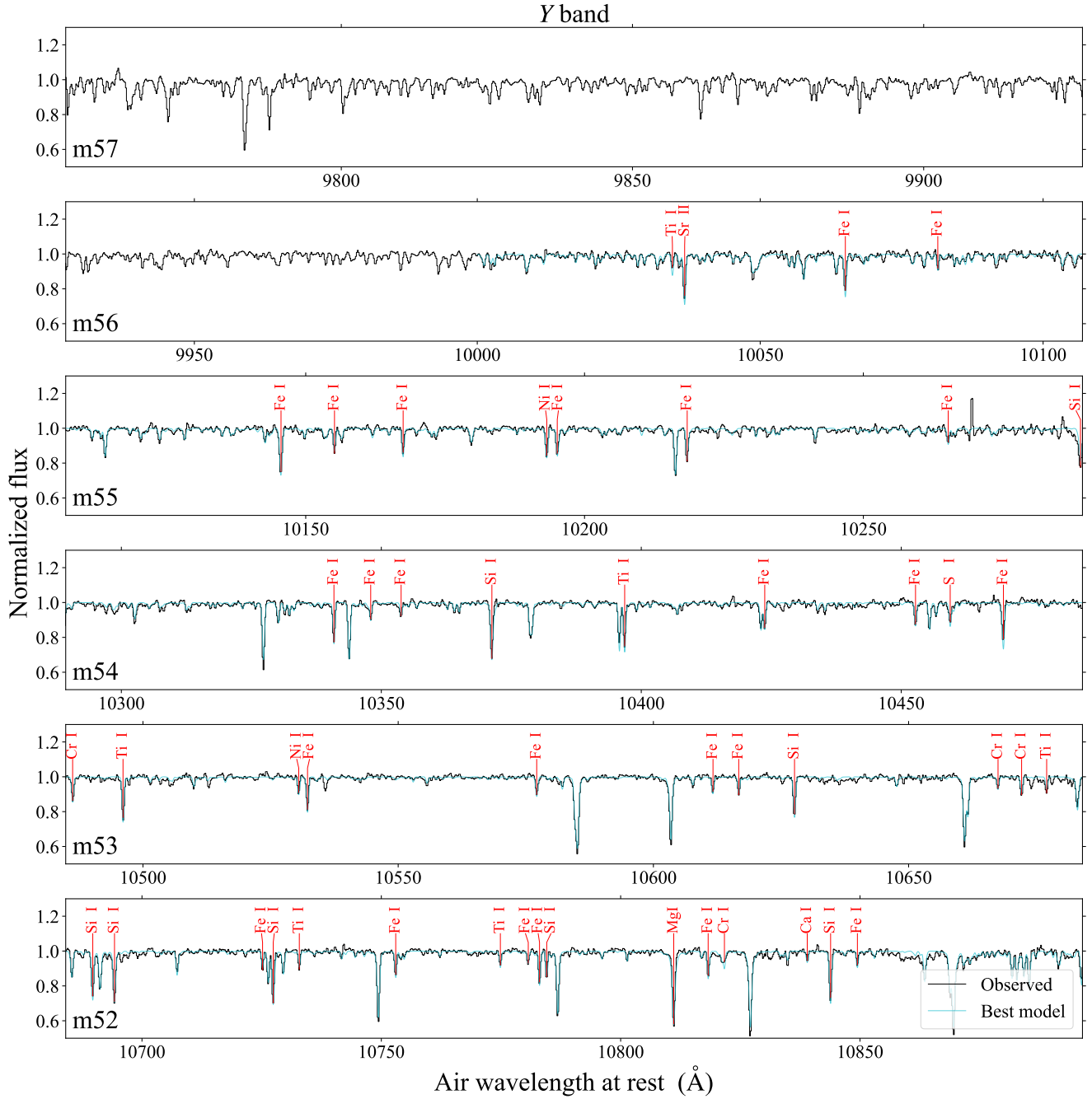


Figure 2. WINERED near-infrared high-resolution spectrum of WINERED-HVS1 in the Y band (echelle orders 57-52). Black lines show the reduced spectrum of WINERED-HVS1, after telluric lines were removed. Cyan lines show the best-fit model spectrum synthesized with the MB99 line list. Red vertical lines near the top edge of each panel mark the wavelengths from the MB99 line list of the lines that were used for measuring $[X/H]$. We note that the MB99 list includes only lines with wavelengths longer than 10,000 \AA , and thus the synthetic spectrum is shown only for wavelengths greater than 10,000 \AA . (The observed and best-fit spectra are available as Data behind the Figure associated with this publication.)

MOOG (Sneden 1973; Sneden et al. 2012). Briefly, we first determined the effective temperature T_{eff} , using the relations between T_{eff} and line-depth ratios (LDRs) of FeI lines calibrated using well-studied red giants by Taniguchi et al. (2021). Following the procedure described by Taniguchi et al. (2025b, in prep.), we removed the systematic bias in the determined T_{eff} due to the metallicity effect on the T_{eff} -LDR relations. In this step, we adopted the metallicity of WINERED-HVS1 of -0.2624 dex, which is the value tabulated in the Gaia DR3 catalog (`mh_gspphot`) after removing the systematic bias in it following the recipe by Andrae et al. (2023b). The amount of the removed bias is 13 K, which is much smaller than the error in the determined T_{eff} , 76 K. Next, we calculated the surface gravity $\log g$ using the Stefan-Boltzmann law with some stellar parameter values: the LDR effective temperature determined here, the mass $M = 1-3M_{\odot}$ estimated in Appendix B, and luminosity $L = 51.06^{+8.22}_{-7.52}L_{\odot}$ tabulated in the Gaia DR3 catalog (`lum_flame`). Then, by fitting some of the FeI lines that are relatively free from the contamination by surrounding lines, we determined v_{micro} and $[\text{Fe}/\text{H}]$ that give no correlation between the line strengths and $[\text{Fe}/\text{H}]$ s determined with the individual lines. Finally, we determined $[\text{X}/\text{H}]$ of Na, Mg, Si, S, K, Ca, Ti, Cr, Ni, and Sr by fitting relatively uncontaminated individual lines of these elements. Throughout the analysis, we used the grid of ATLAS9-APOGEE model atmospheres (Mészáros et al. 2012). We used two line lists, the list with astrophysical $\log gf$ values calibrated against the Sun by Meléndez & Barbuy (1999, MB99) and the Vienna Atomic Line Database (VALD3; Ryabchikova et al. 2015), and compared the results to identify potential differences if any.

In determining $[\text{Fe}/\text{H}]$ and $[\text{X}/\text{H}]$, we employed the so-called differential analysis method (Jofré et al. 2019) to reduce the systematic bias in the determined chemical abundances due to the inaccuracy in infrared line lists (see, e.g., Andreasen et al. 2016; Matsunaga et al. 2020). As the reference stars of the differential analysis, we analyzed the WINERED spectra of two well-investigated thin-disk red giants, ε Vir and Pollux, observed by Taniguchi et al. (2018). The two stars have the stellar parameters and observed spectra similar to those of WINERED-HVS1. Stellar parameters ($[\text{Fe}/\text{H}]$, T_{eff} , $\log g$, and v_{micro}) and chemical abundances of the two reference stars were mainly adopted from the Gaia FGK benchmark stars v2.1 (Jofré et al. 2018). They only determined $[\text{X}/\text{H}]$ of Mg, Si, Ca, Ti, Cr, Fe, and Ni among the elements of our interest, and thus we adopted $[\text{X}/\text{H}]$ of the other elements (Na, S, K, and Sr) from other literature or estimated with an assumption: $[\text{Na}/\text{H}]$ was adopted from the study by Jofré et al. (2015), $[\text{S}/\text{H}]$ and $[\text{K}/\text{H}]$ were estimated assuming $[\text{S}/\text{H}] = [\text{K}/\text{H}] = ([\text{Mg}/\text{H}] + [\text{Si}/\text{H}] + [\text{Ca}/\text{H}])/3$, and $[\text{Sr}/\text{H}]$ was assumed to have the same value as $[\text{Ba}/\text{H}]$ determined by Jofré et al. (2015). Hence, the determined

$[\text{X}/\text{H}]$ of Na, S, K, and Sr for WINERED-HVS1 are possibly subject to a systematic bias in the zero point.

Two sources of errors were considered in the analysis: the standard error of line-by-line dispersion and the errors propagated from the errors in stellar parameters (see equations (9) and (10) in Taniguchi et al. 2025). The errors for most elements are dominated by the standard error of the line-by-line dispersion, but the error propagated from the error in T_{eff} also markedly contribute to some elements (Si, S, Ti, and Cr).

Figure 4 compares the resultant chemical composition of WINERED-HVS1 determined with the MB99 (Table 4) and VALD3 (Table 5) line lists. We found an overall good agreement between the abundances determined with the two lists. Since the MB99 list generally better reproduces near-infrared spectra of late-type stars (Kondo et al. 2019; Taniguchi et al. 2025), we used the results with the MB99 list, presented in Table 4, in the following discussion. For brevity, we only present $[\text{X}/\text{H}]$ and $[\text{X}/\text{Fe}]$ in Table 4. However, our analysis also allows us to obtain abundance ratio between α elements, such as $[\text{Si}/\text{Mg}] = 0.201^{+0.073}_{-0.074}$, $[\text{Ca}/\text{Mg}] = 0.057^{+0.176}_{-0.177}$, and $[\text{Ti}/\text{Mg}] = 0.066^{+0.162}_{-0.170}$. These $[\text{X}/\text{Mg}]$ ratios will turn out to be informative in understanding the origin of WINERED-HVS1.

7. DISCUSSION

In Section 5, we selected 22 metal-rich HVS candidates from the Gaia DR3 catalog. For one of the candidates, WINERED-HVS1, we conducted follow-up observations to obtain the detailed chemical abundances (see Section 6). In this Section, we will first discuss the kinematical (Table 2) and chemical properties (Table 3) of these 22 stars. Then we focus on the most-metal rich candidate, WINERED-HVS1, and discuss its origin.

7.1. Kinematical properties of metal-rich HVS candidates

As mentioned in Section 5.2, we trace the stellar orbit in the last 200 Myr and call the position and velocity at the last disk crossing as the *ejection* position and *ejection* velocity for brevity. While we use them to identify the HVS candidates, in general there is no guarantee that the time at the last disk crossing ($t = -\tau$) corresponds to the time when the star was ejected (from the SMBH). Still, the value of v_{ej} is useful to characterize the HVS ejection, and the orbit since the last disk crossing allows an intuitive understanding of the HVS orbit. In the following, we analyze the orbital properties at $-\tau < t < 0$ for each HVS candidate.

For each metal-rich HVS candidate, we have N_{MC} orbit realizations. By using these Monte Carlo orbits in our fiducial search (i.e., Method A), we select the orbits that satisfy either (Condition 1) or (Condition 2), and then find the ‘best’ orbit that has the smallest ejection radius r_{ej} .

Table 4. Spectroscopic results of WINERED-HVS1

v_{helio} [km s ⁻¹]	34.79 ± 0.13^a		
T_{eff} [K]	4680 ± 76		
$\log g$	2.6 ± 0.2		
v_{micro} [km s ⁻¹]	$1.531^{+0.160}_{-0.150}$		
[Fe/H] [dex]	$-0.147^{+0.046}_{-0.045}$ (43)		
	[X/H] [dex]	[X/Fe] [dex]	
Na I ^b	$-0.203^{+0.272}_{-0.274}$	$-0.056^{+0.272}_{-0.276}$	(1)
Mg I	$-0.205^{+0.048}_{-0.047}$	$-0.058^{+0.077}_{-0.082}$	(5)
Si I	$-0.003^{+0.071}_{-0.068}$	$+0.144^{+0.088}_{-0.091}$	(17)
S I ^b	$+0.036^{+0.334}_{-0.326}$	$+0.182^{+0.342}_{-0.339}$	(1)
K I ^b	$+0.391^{+0.284}_{-0.288}$	$+0.538^{+0.286}_{-0.293}$	(1)
Ca I	$-0.148^{+0.170}_{-0.170}$	$-0.001^{+0.175}_{-0.177}$	(5)
Ti I	$-0.139^{+0.154}_{-0.157}$	$+0.008^{+0.140}_{-0.151}$	(9)
Cr I	$-0.205^{+0.134}_{-0.133}$	$-0.058^{+0.129}_{-0.134}$	(7)
Ni I	$-0.189^{+0.194}_{-0.193}$	$-0.042^{+0.194}_{-0.194}$	(2)
Sr II ^b	$+0.013^{+0.297}_{-0.296}$	$+0.160^{+0.299}_{-0.301}$	(1)

NOTE—Chemical abundances, [X/H] and [X/Fe], were determined using the MB99 line list (Meléndez & Barbuy 1999). The results using the VALD3 list are presented in Table 5. Numbers in brackets show the number of lines analyzed.

^aWith a possible systematic bias of ~ 1.0 km s⁻¹ at most.

^b[Na/H], [S/H], [K/H], and [Sr/H] are possibly subject to a systematic bias in the zero point. See text for details.

The properties of the best orbits of the metal-rich HVS candidates are summarized in Table 2. In Fig. 5, we show the Monte Carlo orbits as well as the best orbit for WINERED-HVS1.¹⁰ Mainly due to the uncertainty in the heliocentric distance to this star, the ejection position of this star is uncertain, as shown in Fig. 5(a). However, the best orbit (shown in Fig. 5(b)) can be traced back to very close to the Galactic center, showing that this star is a candidate of an HVS.¹¹

Table 2 indicates that all of the metal-rich HVS candidates have ejection velocities of $v_{\text{ej}} \simeq 500\text{--}600$ km s⁻¹ in their best orbits. This result suggests that they are bound to the Milky Way, because their v_{ej} values are lower than the escape velocity near the Galactic center (ignoring the gravity from the SMBH Sgr A*), $v_{\text{esc,GC}} \simeq 700\text{--}800$ km s⁻¹.¹² Indeed, one candidate

¹⁰ Orbits for the other HVS candidates are shown in Figs. 12, 13, 14, 15, and 16, in Appendix G.

¹¹ The systematic uncertainty in r_{ej} arising from the specific choice of the Galactic potential is ~ 200 pc (see Section 5.2.1). Thus, if $r_{\text{ej}} \lesssim 200$ pc, the orbits are consistent with the Galactic center origin.

¹² We checked some of the widely used Galactic potential models from literature (McMillan 2017; Piffl et al. 2014; Portail et al.

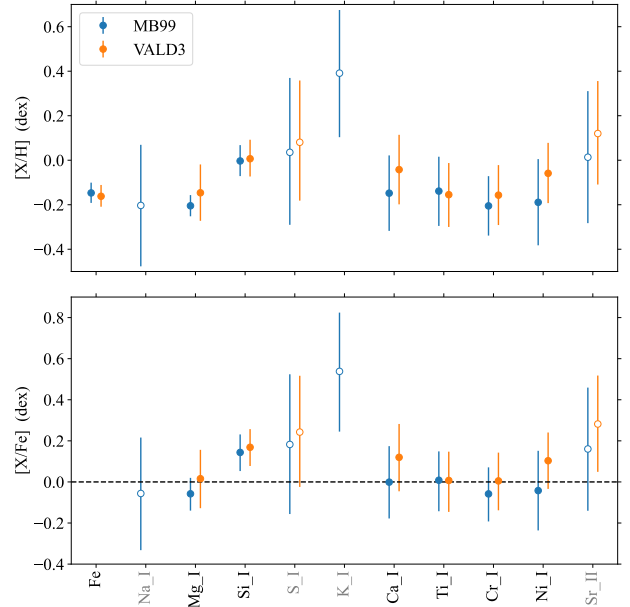


Figure 4. Chemical abundances, [X/H] and [X/Fe], of WINERED-HVS1, summarized in Table 4 (blue; fiducial result using the MB99 line list) and Table 5 (orange; using the VALD3 line list). We employed the differential analysis against two Gaia FGK benchmark stars, ϵ Vir and Pollux. For elements indicated by filled circles, we adopted [X/H] of the reference stars determined by Jofré et al. (2018). In contrast, reference [X/H] of elements indicated by open circles were taken from other literature or estimated with an assumption, and thus they are subject to a possible systematic bias in the zero point. See the main text for more detail.

(mrHVSxp7) has $v_r < 0$ (see Fig. 15), which implies a bound orbit. We stress that, due to the bound nature of these stars, we lack a clear understanding of when exactly these metal-rich HVS candidates were ejected by the SMBH, assuming they are indeed genuine HVSs.

The only unambiguous HVS known to date is S5-HVS1, whose ejection velocity is estimated to be ~ 1800 km s⁻¹ (Koposov et al. 2020). Compared to the ejection velocity of S5-HVS1, the ejection velocities of our metal-rich HVS candidates are considerably smaller. In terms of ejection velocity, our sample does not contain any unambiguous HVS candidates. An independent analysis by Marchetti et al. (2022) also reached the same conclusion (i.e., they did not find unambiguous HVSs in their analysis). However, we note that the ejection velocities of our metal-rich HVS candidates, $500\text{--}600$ km s⁻¹, are consistent with the theoretical predictions for the ejection velocities of HVSs (Bromley et al. 2006; Brown 2015; Marchetti et al. 2018).

Among these models, the one in Portail et al. (2017) has the smallest value of $v_{\text{esc,GC}} = 684$ km s⁻¹.

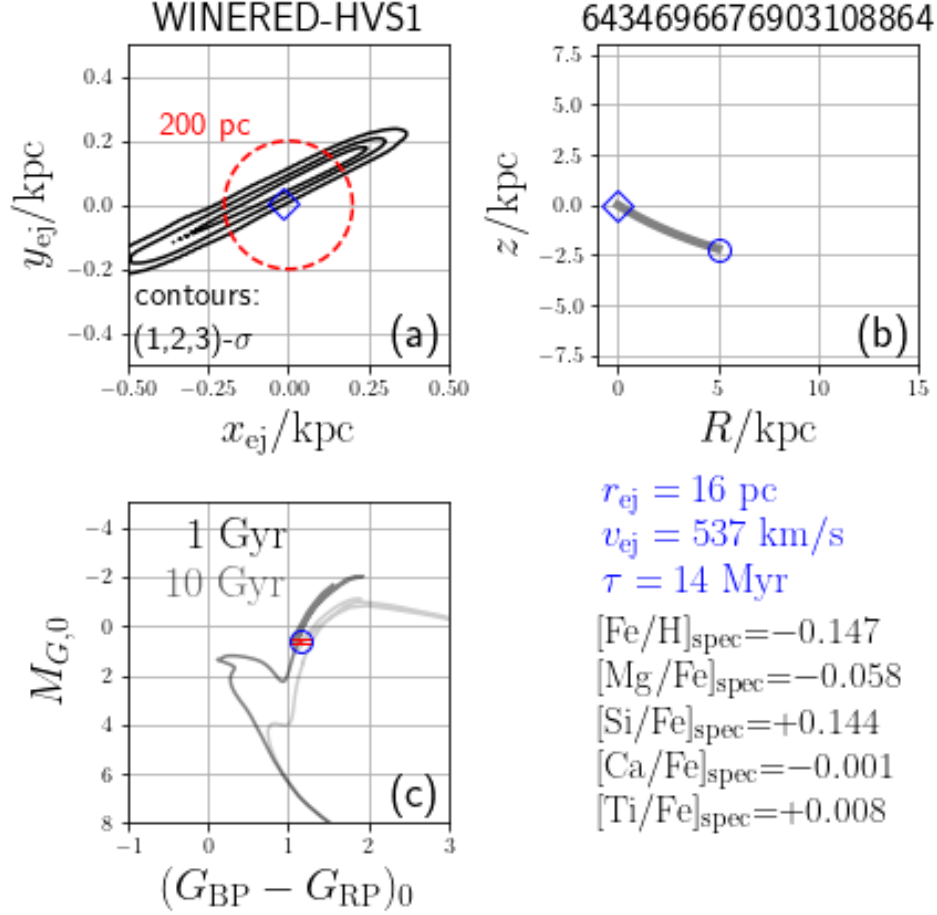


Figure 5. The orbital properties of WINERED-HVS1 (Gaia DR3 6434696676903108864) under the fiducial assumptions (Method A) since the last disk crossing. (a) The intersection of the Monte Carlo orbits with the Galactic disk plane at the last disk crossing, referred to as the ejection position. The three contours enclose 39.3, 86.5, and 98.9 percent of the ejection positions. The open blue diamond indicates the ejection position of the best orbit—the orbit most consistent with a recently-ejected HVS orbit (with the smallest r_{ej}). The red dashed circle indicates a Galactocentric radius of 200 pc, which corresponds to the systematic uncertainty in the ejection position arising from the specific choice of the Galactic potential model. (b) The best orbit in the Galactocentric meridional plane. The current position and the ejection position are marked by an open blue circle and diamond, respectively. The ejection velocity of the best orbit is $v_{ej} = 537 \text{ km s}^{-1}$. If WINERED-HVS1 was recently ejected from the Galactic center, its flight time is 14 Myr. In 5 Myr, the orbit is expected to reach the apocenter at $r = 11.6 \text{ kpc}$. (c) The location of the WINERED-HVS1 in the color-magnitude diagram (CMD). We compute the extinction-corrected color $(G_{BP} - G_{RP})_0$ and absolute magnitude $M_{G,0}$ for each Monte Carlo orbit, as different stellar distance is assumed for each orbit. The blue circle corresponds to the location in the CMD when the best orbit is adopted. The red vertical error bar represents the range of $M_{G,0}$ if its ejection position is within 200 pc of the Galactic center. In correcting for the dust extinction, we use a 3D dust map Combined19 from `mw dust` package (Bovy et al. 2016), in which three 3D dust maps are combined (Drimmel et al. 2003; Marshall et al. 2006; Green et al. 2019). We also plot 1 Gyr and 10 Gyr isochrones from the BaSTI model (Hidalgo et al. 2018), by assuming the stellar metallicity closest to that of this star. The observed properties suggest that WINERED-HVS1 is roughly 0.5–10 Gyr old (see Appendix B).

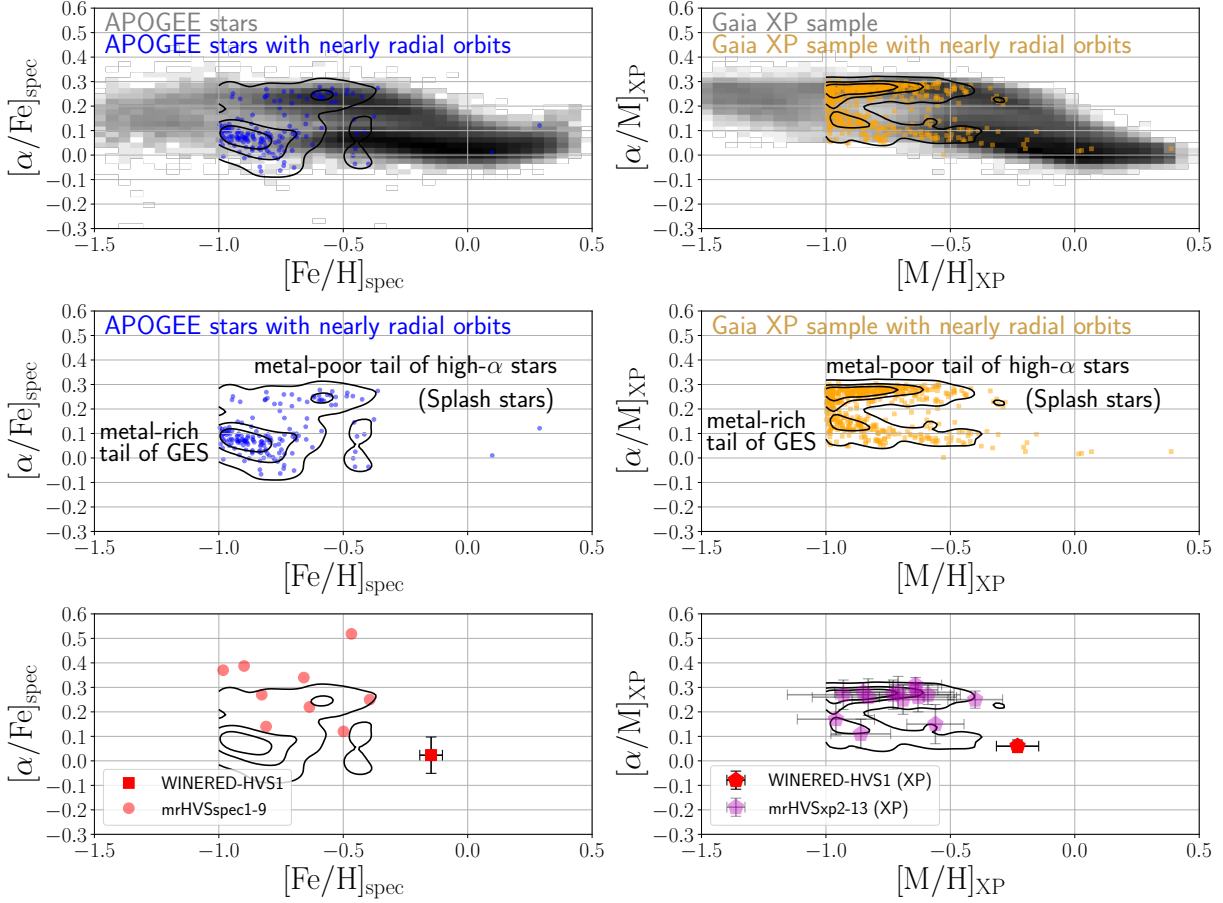


Figure 6. We compare the metallicity and α -abundance of metal-rich stars that exhibit nearly radial orbits (which are presumably non-HVS stars; see [Appendix C](#) for selection criteria) and those of our HVS candidates. (Left Column) We compare the APOGEE stars and our HVS candidates with known spectroscopic abundances (mrHVSspec1-9 and WINERED-HVS1). The distribution of the cleaned sample of APOGEE DR17 stars is shown by a grayscale image in the top panel. A subset of APOGEE stars with nearly radial orbits and $[\text{Fe}/\text{H}]_{\text{spec}} > -1$ is marked with blue dots, accompanied by contours enclosing 25%, 50%, and 90% of these stars. This group consists of two distinct sequences: the metal-rich tail of Gaia Enceladus Sausage (GES) and the metal-poor tail of high- α disk stars. Notably, 99.7% of stars with nearly radial orbits and $[\text{Fe}/\text{H}]_{\text{spec}} > -1$ satisfy $[\text{Fe}/\text{H}]_{\text{spec}} < -0.3$, and our HVS candidates labeled as mrHVSspec1-9 also meet this criterion. WINERED-HVS1 with $[\text{Fe}/\text{H}]_{\text{spec}} = -0.147$ emerges as the most promising candidate, distinguishing itself as a metal-rich outlier. (Right Column) Next, we compare Gaia XP stars with our XP-based metal-rich HVS candidates (mrHVSxp2-13 and WINERED-HVS1). The top and middle panels are the same as in the left column, but using a cleaned sample of stars with reliable Gaia XP chemistry. About 98% of stars with nearly radial orbits and $[\text{M}/\text{H}]_{\text{XP}} > -1$ have $[\text{M}/\text{H}]_{\text{XP}} < -0.3$, and our HVS candidates labeled as mrHVSxp2-13 also meet this condition. WINERED-HVS1 has a metallicity of $[\text{M}/\text{H}]_{\text{XP}} = -0.23$, which is a clear metal-rich outlier, even when assessed through our XP-based metallicity measurements.

7.2. Chemical properties of metal-rich HVS candidates

Since our HVS candidates are bound to the Milky Way (unlike the unambiguous HVS known as S5-HVS1), the orbital properties alone are not informative enough to constrain the origin of these stars. Rather, given the small ejection rate of HVSs (Brown 2015; see also our discussion in Section 1.2), it would not be surprising if most of our candidates were non-HVSs. In this regard, chemical properties of our candidates, which are summarized in Table 3, are important to understand the origin of these stars.

7.2.1. Metallicity and α -abundance

In the left column of Fig. 6, we compare the metallicity and α -abundance of our HVS candidates with spectroscopic abundances (WINERED-HVS1 and mrHVSspec1-9) with a sample of reference stars from APOGEE DR17 (see Appendix C). The top-left and middle-left panels indicate that the APOGEE stars with radial orbits primarily originate from two populations of stars. The first population is the Gaia-Enceladus-Sausage (GES), which is the remnants of the last major merger (Belokurov et al. 2018; Helmi et al. 2018). Because of the near head-on merger of the GES and the ancient Milky Way, the stars originated from GES have nearly radial orbits. The second component is the metal-poor tail of the high- α (disk) stars. This population may be a so-called Splash component, which are the stars in the pre-existing high- α disk that were kicked out of the disk due to the GES merger (Bonaca et al. 2017; Belokurov et al. 2020). These stars may also be kinematically hot tail of the high- α disk stars (see Fig. 15(a)(b) in Hattori 2025). Due to their eccentric orbits, these two populations may contaminate our metal-rich HVS candidates. Most of the radial orbit contaminants have metallicities $[\text{Fe}/\text{H}]_{\text{spec}} < -0.3$. In our selection, we identified 628 APOGEE stars with radial orbits and $[\text{Fe}/\text{H}]_{\text{spec}} > -1$. Notably, among these stars, 626 (99.7%) have $[\text{Fe}/\text{H}]_{\text{spec}} < -0.3$. Our candidates mrHVSspec1-9 exhibit $[\text{Fe}/\text{H}]_{\text{spec}} < -0.3$, similar to the majority of the reference APOGEE sample. Among mrHVSspec1-9, seven of them display high $[\alpha/\text{Fe}]_{\text{spec}} > 0.2$, suggesting they may be metal-poor tail of high- α stars; while two of them show low $[\alpha/\text{Fe}]_{\text{spec}} < 0.2$, indicating that they may belong to the metal-rich tail of the Gaia Enceladus Sausage. (The latter view is supported by the low- $[\text{Al}/\text{Fe}]$ of these two stars, as we will discuss in Section 7.2.2.) These results indicate that our candidates mrHVSspec1-9 are consistent with the majority of non-HVS reference stars, possibly associated with GES (mrHVSspec2-3) or Splash (mrHVSspec1 and mrHVSspec4-9). Among the 628 APOGEE stars, only 2 stars (0.3%) have

$[\text{Fe}/\text{H}]_{\text{spec}} > -0.3$,¹³ which indicates that it is very rare to find a non-HVS with high metallicity and low α -abundance. This result provides a supporting evidence that WINERED-HVS1, which shows an exceptionally high metallicity, is an HVS ejected from the Galactic center. (Indeed, as we will discuss in Section 7.4, the detailed chemical abundances of this star are consistent with the Galactic center population.)

In the right column of Fig. 6, we compare the chemistry of XP-based metal-rich HVS candidates with a sample of (non-HVS) stars with reliable $([\text{M}/\text{H}]_{\text{XP}}, [\alpha/\text{M}]_{\text{XP}})$ (see Appendix C). The top-right and middle-right panels confirm the presence of the same two populations of non-HVS stars with nearly radial orbits in the Gaia XP sample.¹⁴ Again, the XP-based metal-rich HVS candidates show $[\text{Fe}/\text{H}]_{\text{spec}} < -0.3$, except for WINERED-HVS1. In terms of the $[\alpha/\text{M}]_{\text{XP}}$ value, mrHVSxp3,9,13 may be possibly associated with the GES component, while mrHVSxp2,4-8,10-12 may be possibly associated with the Splash component.

Based on the distribution of stars in the metallicity and α -abundance space, we conclude that

- WINERED-HVS1 is the most promising candidate for an HVS ejected from the Galactic center (see also Section 7.4).

The other metal-rich HVS candidates (mrHVSspec1-9 and mrHVSxp2-13) are less attractive, but we do not have strong evidence to conclude that they are non-HVSs. However, if we assume—as a working hypothesis—that they are non-HVSs, then our best guess for their origins are as follows:

- mrHVSspec2-3 (see also Section 7.2.2) and mrHVSxp3,9,13 are possibly metal-rich tail of GES stars;
- mrHVSspec1,4-9 and mrHVSxp2,4-8,10-12 are possibly metal-poor tail of Splash stars.

Under this working hypothesis, we only find one HVS (candidate) from our Gaia DR3 catalog with Gaia XP spectra. The statistical implication of this result is discussed in Appendix F.

¹³ These two stars do not exhibit HVS-like orbits.

¹⁴ In the reference APOGEE sample (blue dots in the middle-left panel in Fig. 6), we see more GES-like stars than Splash-like stars. In contrast, in the reference Gaia XP sample (orange dots in the middle-right panel in Fig. 6), we see more Splash-like stars than GES-like stars. We do not fully understand the origin for this difference, but it may be due to the sample selection effect, such that we see low Galactic latitude region for the APOGEE sample and we see high Galactic latitude region (with low dust extinction; Hattori 2025) for the Gaia XP sample. In this regard, it is interesting to point out that our candidates mrHVSspec1-9 and mrHVSxp2-13 are selected from the catalog of Hattori (2025), and we see more Splash-like HVS candidates than GES-like HVS candidates, similar to the distribution of orange dots in the middle-right panel in Fig. 6.

7.2.2. $[Al/Fe]$ -abundance

In understanding the origin of HVS candidates, the abundance ratio of $[Al/Fe]$ is also informative. As we discussed earlier, one of the sources of contamination to the HVSs is the GES, which dominates the stellar halo within 20 kpc from the Galactic center. A distinct feature of GES stars is that they typically show negative $[Al/Fe]$ (Feuillet et al. 2021), unlike other Milky Way stars such as thin disk, thick disk, or bulge stars (Das et al. 2020; Feuillet et al. 2022; Barbuy et al. 2023; Nandakumar et al. 2024). Therefore, the $[Al/Fe]$ ratio is informative to flag possible GES stars.

Among 22 HVS candidates, we have $[Al/Fe]$ measurements for 7 stars, and two stars (mrHVSspec2 and mrHVSspec3) have $[Al/Fe] \lesssim -0.2$ (see Table 3). The $[Al/Fe]$ values of these stars indicate that mrHVSspec2 and mrHVSspec3 are consistent with GES stars.¹⁵ Intriguingly, these two stars have $[\alpha/Fe]_{\text{spec}} = 0.14$ and 0.12, respectively, and have the lowest $[\alpha/Fe]_{\text{spec}}$ among mrHVSspec1-9. In the $([Fe/H]_{\text{spec}}, [\alpha/Fe]_{\text{spec}})$ -space, these stars lie almost along the sequence of the metal-rich tail of the GES stars (see the lower-left panel of Fig. 6). Both $[Al/Fe]$ and $[\alpha/Fe]_{\text{spec}}$ indicate that mrHVSspec2 and mrHVSspec3 are consistent with GES stars. However, we stress that this argument needs to be handled with care, because currently we do not know the $[Al/Fe]$ ratio for any stars in the Galactic center. For example, if future observations indicate that Galactic center stars show low- $[Al/Fe]$, each of mrHVSspec2 and mrHVSspec3 can be considered a good candidate for either an HVS or a GES star.

7.3. Orbital properties of WINERED-HVS1

As discussed in Section 7.2, the high-metallicity and low- $[\alpha/Fe]$ nature of WINERED-HVS1 makes it the most promising HVS candidate. However, its $[\alpha/Fe]$ is also similar to that of the thin disk (low- α) stars (see top panels in Fig. 6). Here we investigate the orbit of WINERED-HVS1 to understand its origin.

7.3.1. Ejection of WINERED-HVS1 from the Galactic disk

So far, we have focused on the orbits in the last 200 Myr and selected HVS candidates whose last disk crossings occurred near the Galactic center. In this section, we adopt a longer integration time of 10 Gyr and explore the past orbit of WINERED-HVS1, to assess the possibility that this star was not ejected by the SMBH but ejected elsewhere in the Galactic disk. To this end, we focus on the best orbit of WINERED-HVS1 (evaluated with Method A) shown in Fig. 5(b). The adopted

integration time (10 Gyr) is motivated by its stellar age (0.5–10 Gyr; see Appendix B).

At each disk-crossing event, we record the disk-crossing time t_{ej} , position \mathbf{x}_{ej} and velocity \mathbf{v}_{ej} , as in Section 5.1. Since we are interested in the Galactic disk ejection, we derive the intrinsic ejection velocity

$$\mathbf{v}_{\text{ej}}^{\text{intrinsic}} = \mathbf{v}_{\text{ej}} - \mathbf{v}_{\text{circ}}(\mathbf{x}_{\text{ej}}), \quad (5)$$

where \mathbf{v}_{circ} corresponds to the velocity of a circular orbit at \mathbf{x}_{ej} . This intrinsic ejection velocity represents the disk ejection velocity corrected for the streaming motion of the disk (see Hattori et al. 2019). (For example, if the star was ejected from a star cluster in the disk, $\mathbf{v}_{\text{ej}}^{\text{intrinsic}}$ is the ejection velocity relative to the cluster.)

Fig. 7 shows the disk crossings of the best orbit of WINERED-HVS1 in the last 10 Gyr. The vertical axis represents the intrinsic ejection velocity $v_{\text{ej}}^{\text{intrinsic}} = |\mathbf{v}_{\text{ej}}^{\text{intrinsic}}|$, and the horizontal axis represents the Galactocentric radius at each disk crossing ($R = |\mathbf{x}_{\text{ej}}|$). Since the orbit has a nearly zero azimuthal angular momentum and we adopt a static and axisymmetric Galactic potential (McMillan 2017), we see a clear sequence of $v_{\text{ej}}^{\text{intrinsic}}$ as a function of R . This sequence has a monotonically decreasing profile, which has a maximum near $R = 0$ kpc and is truncated at the apocenter of this orbit, $R = R_{\text{apo}} \simeq 11.6$ kpc. At the last disk crossing event (14 Myr ago), the orbit crossed the disk plane near the Galactic center as described in Fig. 5. Over the past 10 Gyr, the orbit crossed within 200 pc from the Galactic center 15 times. At these disk crossings, the values of $v_{\text{ej}}^{\text{intrinsic}}$ (and v_{ej}) are nearly identical, and satisfy $v_{\text{ej}}^{\text{intrinsic}} \simeq v_{\text{ej}} \gtrsim 500 \text{ km s}^{-1}$.

Since $v_{\text{ej}}^{\text{intrinsic}}(R)$ is well-behaved, we focus on the disk crossing events that occurred in the last 0.5 Gyr, marked by red pluses in Fig. 7. We note that 0.5 Gyr corresponds to the lower bound for WINERED-HVS1’s age. As shown in the figure, the orbit could have crossed the disk plane 7 times in the past 0.5 Gyr (if the star was ejected more than 0.5 Gyr ago). Disk crossings (1) and (6) in the figure occurred near the Galactic center and show $v_{\text{ej}}^{\text{intrinsic}} > 500 \text{ km s}^{-1}$. In contrast, disk crossings (2), (5), and (7) occurred at $6.8 \text{ kpc} \lesssim R \lesssim 11.5 \text{ kpc}$ and show $240 \text{ km s}^{-1} \lesssim v_{\text{ej}}^{\text{intrinsic}} \lesssim 340 \text{ km s}^{-1}$. These findings suggest that, if this star was ejected from the outer part of the disk, the required ejection velocity would be relatively small.

In general, a disk star can be ejected either by a ‘binary ejection mechanism’ through the supernova explosion of the binary companion, or by the ‘dynamical ejection mechanism’ through a few-body (i.e., 3- or 4-body) interaction. Although the ejection of a $1\text{--}3M_{\odot}$ star (such as WINERED-HVS1) with $v_{\text{ej}}^{\text{intrinsic}} > 500 \text{ km s}^{-1}$ is only possible in idealized environments, ejection with $v_{\text{ej}}^{\text{intrinsic}} = 200\text{--}400 \text{ km s}^{-1}$ is viable through both binary ejection (Tauris 2015) and dynamical ejection (Leonard 1991; Perets & Šubr 2012).

¹⁵ Since we do not know the $[Al/Fe]$ of stars in the immediate neighbor of the SMBH, low- $[Al/Fe]$ nature of these stars does not necessarily mean that they are non-HVSs. However, their low- $[Al/Fe]$ nature does flag that they may be GES stars.

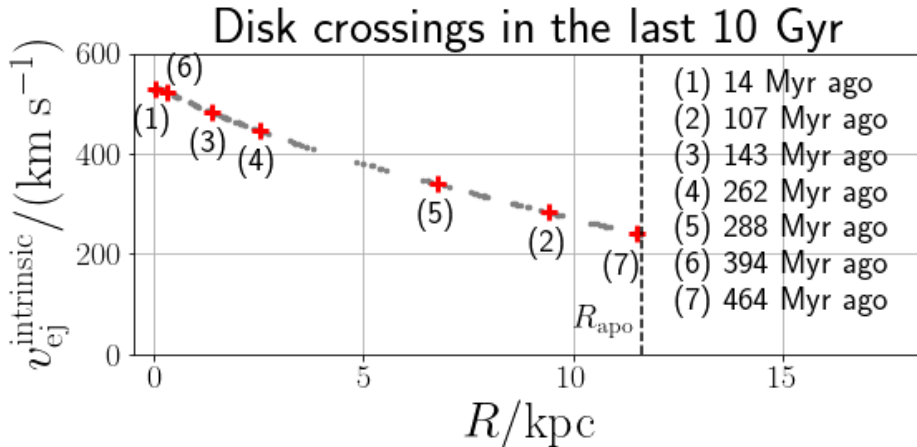


Figure 7. Disk crossings of the best orbit of WINERED-HVS1 in the last 10 Gyr. The x -axis shows the Galactocentric radius R of the disk-crossing positions. The y -axis shows the disk-crossing velocity corrected for the streaming motion of the disk, $v_{\text{ej}}^{\text{intrinsic}}$. Gray dots represent disk crossings in the last 10 Gyr. Red pluses (+) represent disk crossings in the last 0.5 Gyr, enumerated according to the disk-crossing time. The vertical dashed line corresponds to the apocenter radius of the orbit, beyond which disk crossings do not occur. From this analysis, we see that low-velocity ejection ($v_{\text{ej}}^{\text{intrinsic}} = 200\text{--}400 \text{ km s}^{-1}$) from the outer disk can kinematically explain the origin of WINERED-HVS1. (However, see also Fig. 8.)

In this regard, the ejection of WINERED-HVS1 from the (outer) Galactic disk might provide an alternative explanation for the origin of this star. If we hypothesize that the star was ejected from the Galactic disk, we would expect it to share chemical similarities with disk stars. To test this hypothesis, we compared the detailed chemical abundances of this star with those of disk stars. Fig. 8 shows the distribution of chemical abundances of red giant disk stars located at $|z| < 0.5 \text{ kpc}$ from the disk plane. The top panel indicates that the $[\text{Fe}/\text{H}]$ and $[\text{Mg}/\text{Fe}]$ values of WINERED-HVS1 are consistent with those of low- α disk stars, although its $[\text{Mg}/\text{Fe}]$ is slightly lower than that of typical low- α disk stars. In contrast, the bottom panel shows that WINERED-HVS1 has notably higher $[\text{Si}/\text{Mg}]$ than the disk stars. This difference persists even when we further select disk stars based on their Galactocentric radius. These findings indicate that the chemical properties of WINERED-HVS1 are distinct from those of disk stars, suggesting that it was not ejected from the Galactic disk. For reference, Fig. 8 also shows the chemical abundances of NSC stars. We find a chemical similarity between the NSC stars and WINERED-HVS1, which will be further discussed in Section 7.4 and Fig. 10.

7.3.2. Ejection of WINERED-HVS1 from the Galactic center

Here we investigate the physical conditions under which WINERED-HVS1 could have been ejected from the Galactic center. Since the ejection velocity v_{ej} does not depend on the flight time (as long as the Galactic potential is nearly static), we once again use the 10^4 Monte Carlo orbits in the last 200 Myr in this section.

Fig. 9 shows the distribution of the ejection position ($x_{\text{ej}}, y_{\text{ej}}$) of the Monte Carlo orbits of WINERED-HVS1, color-coded by the ejection velocity v_{ej} . Since the Galactic potential is deeper at smaller Galactocentric radius, v_{ej} tends to be larger for smaller r_{ej} . The value of v_{ej} range from 481 km s^{-1} to 539 km s^{-1} ; while the best orbit has an ejection velocity of $v_{\text{ej}} = 537 \text{ km s}^{-1}$.

In Appendix E, we conduct Monte Carlo simulations of HVSs with ejection velocities of $v_{\text{ej}} \simeq 500\text{--}600 \text{ km s}^{-1}$ arising from disrupted binary systems through Hills mechanism. We find that the ejection of WINERED-HVS1 can be reproduced if the semi-major axis a and the periastron distance r_{peri} of the progenitor binary fall within a reasonable range, namely $a \simeq 0.5\text{--}4 \text{ AU}$ and $r_{\text{peri}} \simeq 30\text{--}300 \text{ AU}$ (see Fig. 11).

The ejection of WINERED-HVS1 can be explained by two scenarios: (i) it was ejected as a red giant; or (ii) it was ejected as a main-sequence star which later evolved into a red giant. In the case (i), it may or may not be a recently-ejected HVS. If this star is a recently-ejected HVS, its flight time is $\sim 14 \text{ Myr}$. In the case (ii), it may not be a recently-ejected HVS. This is because a main-sequence star with a mass of $1\text{--}3M_{\odot}$ requires more than 20 Myr to evolve into a red giant similar to WINERED-HVS1. This timescale exceeds the time since the last disk crossing (14 Myr), implying that the star must have undergone at least one, and possibly multiple, disk crossings after ejection (see Appendix E.3).

To summarize, the ejection of WINERED-HVS1 by the SMBH is a viable scenario, which is reassuring since we are searching for HVSs ejected from the Galactic center. In the following section, we discuss the origin of WINERED-HVS1 from a chemical perspective.

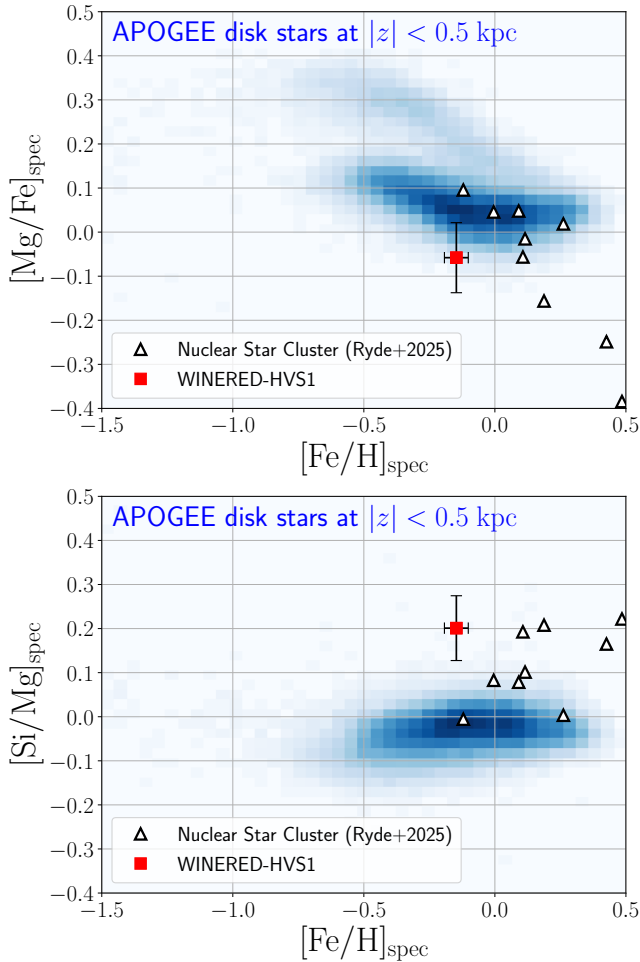


Figure 8. The chemistry of WINERED-HVS1 (red data point) and the APOGEE red giant disk stars (blue density map; see Appendix D). For reference, the chemistry of NSC stars (Ryde et al. 2025) is shown by black triangles. The $[\text{Mg}/\text{Fe}]$ abundance of WINERED-HVS1 is consistent with the low- α disk, but its $[\text{Si}/\text{Mg}]$ ratio differs significantly, indicating that this star was not ejected from the Galactic disk.

7.4. Chemistry of WINERED-HVS1 compared to other stars in the Milky Way and beyond

Here we compare the chemistry of WINERED-HVS1 with that of stars in the NSC, NSD, inner bulge, and dwarf galaxies. Throughout this section, we utilize $[X/Y]$ instead of $[X/Y]_{\text{spec}}$ for brevity, since we only deal with spectroscopically determined chemical abundances.

(1) Nuclear Star Cluster (NSC)

The SMBH at the center of the Milky Way is surrounded by a dense star cluster known as the NSC, whose radius is $\simeq 4$ pc (Schödel et al. 2014). According to the Hills mechanism, when the SMBH disrupts a binary star system at a typical radius of ~ 100 AU $\simeq 5 \times 10^{-4}$ pc, it ejects one star as an HVS while capturing the companion star as an S-star. Since HVS ejections

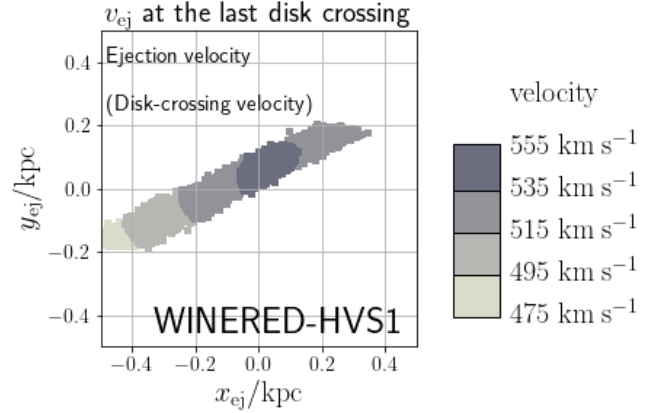


Figure 9. The ejection velocity (disk-crossing velocity) v_{ej} of WINERED-HVS1 as a function of the ejection position $(x_{\text{ej}}, y_{\text{ej}})$ for our 10^4 Monte Carlo orbits evaluated with Method A. Here we only consider the last disk crossing, which occurred ~ 14 Myr ago. Based on these results, we infer that the ejection velocity of WINERED-HVS1 is around $v_{\text{ej}} \simeq 500\text{--}600$ km s^{-1} if it originated from the Galactic center.

occur at the central part of the NSC, we expect a chemical similarity between HVSs and NSC stars.

The observed chemical abundances for NSC stars (including an S-star) are summarized in the left column of Fig. 10. As seen from the metallicity distribution of the NSC stars (bottom panel; Feldmeier-Krause et al. 2020; Do et al. 2015), the majority of stars in the NSC have super-solar metallicity, while more than $\sim 10\%$ of the stars show sub-solar metallicity. The observed metallicity of $[\text{Fe}/\text{H}] = -0.147$ for WINERED-HVS1 is within the metallicity range of NSC stars. Also, the values of $[\alpha/\text{Fe}]$, $[\text{Mg}/\text{Fe}]$, $[\text{Si}/\text{Mg}]$, and $[\text{Ca}/\text{Mg}]$ for WINERED-HVS1 are within the range of the nine NSC red giants at 0.3–4 pc from the SMBH analyzed by Ryde et al. (2025) (black open diamonds). Therefore, broadly speaking, the chemistry of WINERED-HVS1 is consistent with that of NSC stars. Of course, a more detailed comparison with larger number of NSC stars is required to support this view. For example, the nine red giant stars analyzed by Ryde et al. (2025) include two stars with solar or slightly sub-solar $[\text{Fe}/\text{H}]$. Although these two stars have similar metallicity to WINERED-HVS1, they have slightly higher $[\text{Mg}/\text{Fe}]$ and slightly lower $[\text{Si}/\text{Mg}]$ than WINERED-HVS1. It is unclear if these differences are serious or benign, especially because (i) we have only two NSC stars to make a comparison; (ii) $[\text{Mg}/\text{Fe}]$ and $[\text{Si}/\text{Mg}]$ for the NSC stars and WINERED-HVS1 are associated with non-negligible uncertainties (~ 0.1 dex); and (iii) these two stars and WINERED-HVS1 are observed and analyzed in a different manner, and hence subject to a possible systematic bias in the zero point.

The blue upside-down triangle in the left column of Fig. 10 shows the chemistry of S0-6/S10. This star is

the only S-star for which detailed chemistry is known (Nishiyama et al. 2024), and its projected distance from the SMBH is only 0.012 pc. The chemistry of the nine NSC stars in Ryde et al. (2025) is not particularly similar to that of S0-6/S10, although these nine red giants, along with the S0-6/S10, are all located within the NSC. This difference might indicate the chemical inhomogeneity within the NSC (Feldmeier-Krause et al. 2020). Intriguingly, in the $([\text{Fe}/\text{H}], [\text{Mg}/\text{Fe}])$ -space, WINERED-HVS1 is located in between the S0-6/S10 and the sample in Ryde et al. (2025). Since we only have one S-star and one HVS candidate, we can not draw a useful conclusion as to whether the HVSs and S-stars have similar chemical properties as a population.

(2) Nuclear Stellar Disk (NSD)

NSD is a rotationally supported stellar disk at $R \lesssim 220$ pc (Nishiyama et al. 2013; Schultheis et al. 2021). Feldmeier-Krause (2022) studied the chemical abundances of stars within the NSD to find that NSC and NSD show different chemistry, such that NSD stars are typically more metal-poor than NSC stars.

The chemical properties of NSD is summarized in the second column in Fig. 10. The black filled circles show the NSD stars analyzed by Ryde et al. (2016b). The open gray circles show the NSD stars in APOGEE selected by Schultheis et al. (2020). In the original study of Schultheis et al. (2020), they used the chemical abundances in APOGEE DR16, while in this figure we adopt the more recent values from APOGEE DR17. The cyan circle is a metal-poor NSD star known as GC10812,¹⁶ whose metallicity almost corresponds to the lowest metallicity of the NSD sample in Schultheis et al. (2020). The two NSD samples from Ryde et al. (2025) and Schultheis et al. (2020) show a broadly consistent profiles of $[\alpha/\text{Fe}]$, $[\text{Mg}/\text{Fe}]$ and $[\text{Si}/\text{Mg}]$ as a function of $[\text{Fe}/\text{H}]$. Notably, the value of $[\text{Si}/\text{Mg}]$ for the sample in Schultheis et al. (2020) is almost insensitive to $[\text{Fe}/\text{H}]$. This trend is also true for the sample of Ryde et al. (2016b), although we see a larger scatter for this sample. Interestingly, the low- $[\text{Si}/\text{Mg}]$ nature of the NSD stars seems to be inconsistent with the high $[\text{Si}/\text{Mg}]$ ratio observed for WINERED-HVS1. Also, the observed $[\text{Mg}/\text{Fe}]$ ratio of WINERED-HVS1 is slightly smaller than $[\text{Mg}/\text{Fe}]$ of both Ryde et al. (2016b) sample and Schultheis et al. (2020) sample. The offset in $[\text{Si}/\text{Mg}]$ (and a marginal offset in $[\text{Mg}/\text{Fe}]$) may indicate that the WINERED-HVS1 is not chemically consistent with the stellar population in the NSD.

(3) Inner bulge

We further investigate the chemical properties of the inner bulge (at $R \lesssim 300$ pc), which are shown in the third column of Fig. 10. Here, the black plus and or-

ange cross correspond to the inner bulge samples taken from Nandakumar et al. (2024) and Ryde et al. (2016b), respectively. Most notably, the inner bulge stars show low values of $[\text{Si}/\text{Mg}]$, which is in contrast to the high $[\text{Si}/\text{Mg}]$ ratio seen in WINERED-HVS1. This discrepancy indicates that the WINERED-HVS1 is chemically distinct from inner bulge stars.

(4) Dwarf galaxies

The $[\text{Fe}/\text{H}]$ and $[\alpha/\text{Fe}]$ of WINERED-HVS1 resembles that of stars found at the metal-rich end of massive dwarf galaxies. Motivated by this fact, we compare WINERED-HVS1 with stars in dwarf galaxies and GES (remnants of a disrupted dwarf galaxy). In the rightmost column in Fig. 10, we show the chemical properties of stars in the LMC (pink ‘L’; Van der Swaelmen et al. 2013), Sagittarius dwarf galaxy (purple ‘S’; Minelli et al. 2021), and the GES (green ‘G’; see Appendix C).

The stars in the GES are not as metal-rich as WINERED-HVS1, possibly due to the quenched star formation in the GES when it merged to the Milky Way (Ernandes et al. 2024). The chemistry of GES stars indicates that WINERED-HVS1 is not a GES star.

The other massive, surviving dwarf galaxies in this plot (LMC and Sagittarius) are large enough to maintain star formation activity for a long duration of time. Therefore, some stars located in the central part of the LMC and Sagittarius dwarf galaxy are as metal-rich as WINERED-HVS1. For example, the Sagittarius dwarf galaxy has a NSC known as M54 (Alfaro-Cuello et al. 2019), in which young (~ 1 Gyr old) and metal-rich stars are confirmed. Although WINERED-HVS1 is metal-rich, it is unclear if this star is as young as ~ 1 Gyr old. (Our current guess of its age is 0.5–10 Gyr based on the CMD in Fig. 5 and quite uncertain.) However, if WINERED-HVS1 is indeed young, we see a similarity between WINERED-HVS1 and the metal-rich stars in massive dwarf galaxies. In such a case, WINERED-HVS1 might have formed in the NSC of a massive dwarf galaxy. If this star was formed in the NSC of a massive dwarf galaxy, and yet it was ejected from the Galactic center, we need to speculate a scenario to bring this star from its progenitor dwarf galaxy to the Galactic center.

It is unrealistic to suggest that this star was formed in the Sagittarius (or LMC) and was later brought to the Milky Way’s NSC because the apocenter distance of this star is too small to have originated from these surviving dwarf galaxies. Therefore, it is more likely that WINERED-HVS1 was formed in the NSC of a hypothetical massive dwarf galaxy that later merged with the Milky Way. If this hypothetical dwarf galaxy was massive enough to host an NSC, the dynamical friction might have brought the dwarf galaxy and its NSC to

¹⁶ The projected distance of this star from the SMBH is 1.5 pc, but Ryde et al. (2016a) and Ryde et al. (2025) interpret this star as a NSD star, based on its kinematics and photometric information.

the Galactic center. Then the dwarf galaxy’s NSC can merge with the Milky Way’s NSC.¹⁷

If WINERED-HVS1 was formed before the NSC merger, it could reflect the chemistry of the dwarf galaxy’s NSC. Also, if WINERED-HVS1 was brought to the center of the Milky Way’s NSC, it could be ejected as a Galactic HVS. Indeed, the Milky Way’s NSC exhibits an asymmetric spatial distribution of sub-solar metallicity stars (Feldmeier-Krause et al. 2020), which can be interpreted as a result of the merger of NSCs within the last ~ 3 Gyr—a time frame recent enough to retain the dynamical relics (Arca Sedda et al. 2020).

There are several caveats to our scenario. If the merger with this hypothetical dwarf galaxy occurred recently and if that dwarf galaxy was sufficiently massive to host an NSC, we should expect to see the stellar stream of its merger debris in the halo. Thus, the merger must have happened a long time ago (~ 10 Gyr). In this context, a hypothetical dwarf galaxy known as Kraken (also known as Heracles), which is a dwarf galaxy with a stellar mass of $\sim 10^9 M_\odot$ claimed to contribute to the central part of the Milky Way (Kruijssen et al. 2019; Horta et al. 2021), might be a good candidate for the progenitor dwarf galaxy of WINERED-HVS1. Although the Kraken dwarf galaxy is predominantly composed of metal-poor and high- α stars ($[\text{Fe}/\text{H}] \simeq -1$ and $[\text{Mg}/\text{Fe}] \simeq 0.3$; Horta et al. 2023), its NSC could be as metal-rich and low- α as WINERED-HVS1.

Assuming the progenitor dwarf galaxy (possibly Kraken) merged with the Milky Way ~ 10 Gyr ago, we need to explore a mechanism that would gradually bring its NSC to the Galactic center over a timescale of ~ 7 Gyr (if we presume the NSC merger occurred 3 Gyr ago). According to the simulations in Arca Sedda et al. (2020), some models classified as ‘late infalls’ satisfy this condition. Therefore, while not entirely convincing, it may be possible for WINERED-HVS1 to have formed in the NSC of a massive dwarf galaxy and been ejected from the Galactic center.

¹⁷ If this scenario holds true, it is possible to propose an alternative scenario in which WINERED-HVS1 was formed in a Young Massive Cluster (Portegies Zwart et al. 2010) within the stellar disk. If the progenitor cluster was later dragged to the Galactic center due to the dynamical friction and merged to the NSC, WINERED-HVS1 could be ejected by the SMBH. However, this scenario cannot account for the origin of WINERED-HVS1, as stars in Young Massive Clusters typically exhibit chemistry similar to that of low- α disk stars, which is characterized by a low value of $[\text{Si}/\text{Mg}]$ (see Fig. 8) and inconsistent with the high value of $[\text{Si}/\text{Mg}] = 0.201^{+0.073}_{-0.074}$ for this star.

More detailed chemical abundances of WINERED-HVS1, such as its abundances of r -process elements, are required to fully understand its birth environment.¹⁸

7.5. Future prospect

7.5.1. Use of other large catalogs

In this work, we use the catalog of chemical abundances in Hattori (2025) to search for metal-rich HVSs, because it is the largest catalog containing both $[\text{M}/\text{H}]_{\text{XP}}$ and $[\alpha/\text{M}]_{\text{XP}}$. In the hindsight, however, the metallicity data is more important than α -abundance data in identifying HVS candidates. Thus, it may be beneficial to utilize existing large catalogs of metallicity, such as those by Andrae et al. (2023a) and Zhang et al. (2023). This approach could help in identifying metal-rich HVS candidates, even if the catalogs do not include α -abundance information.

Several stellar surveys, including WEAVE (Jin et al. 2023), 4MOST (de Jong et al. 2019), and PFS (Takada et al. 2014), are measuring the line-of-sight velocities for millions of stars. These new catalogs will allow us identify more HVS candidates.

7.5.2. Longer integration time

In this paper, we focused on the stellar orbits in the last 200 Myr to minimize orbital uncertainties. However, since we may have missed some HVSs whose last disk crossings occurred far from the Galactic center, it could be interesting to search for other bound HVSs by adopting a longer integration time.

7.5.3. Optical view of the Galactic center environment using hyper-velocity stars

In Section 6, we use the near-infrared YJ -band spectrum to derive the chemical abundances of WINERED-HVS1. As this star is moving in the halo region (see Fig. 5), where dust extinction is minimal, we can obtain an optical spectrum for this star. The optical spectrum contains absorption lines of several heavy elements (such as Eu and other r -process elements) that are not available in an infrared spectrum with measurable strengths. By analyzing the chemical abundances of WINERED-HVS1 from its optical spectrum, we may gain insights into the chemical landscape near the Galactic center.

Traditionally, understanding the Galactic center environment has been challenging due to the high levels

¹⁸ In this context, it is important to mention the work by Nishiyama et al. (2024). According to their study, the S-star known as S0-6/S10 is more than 10 Gyr old and its $[\text{Fe}/\text{H}]$ and $[\alpha/\text{Fe}]$ are similar to some metal-rich stars in massive dwarf galaxies such as LMC and Sagittarius. We note that metal-rich stars in massive dwarf galaxies have a relatively young age (~ 1 Gyr old), and therefore stars like S0-6/S10, namely old and metal-rich stars, cannot be formed in large dwarf galaxies. For our HVS candidate WINERED-HVS1, the stellar age is around 0.5–10 Gyr. Thus, in case it is young (~ 1 Gyr old), this star could be more or less similar to the metal-rich stars in massive dwarf galaxies.

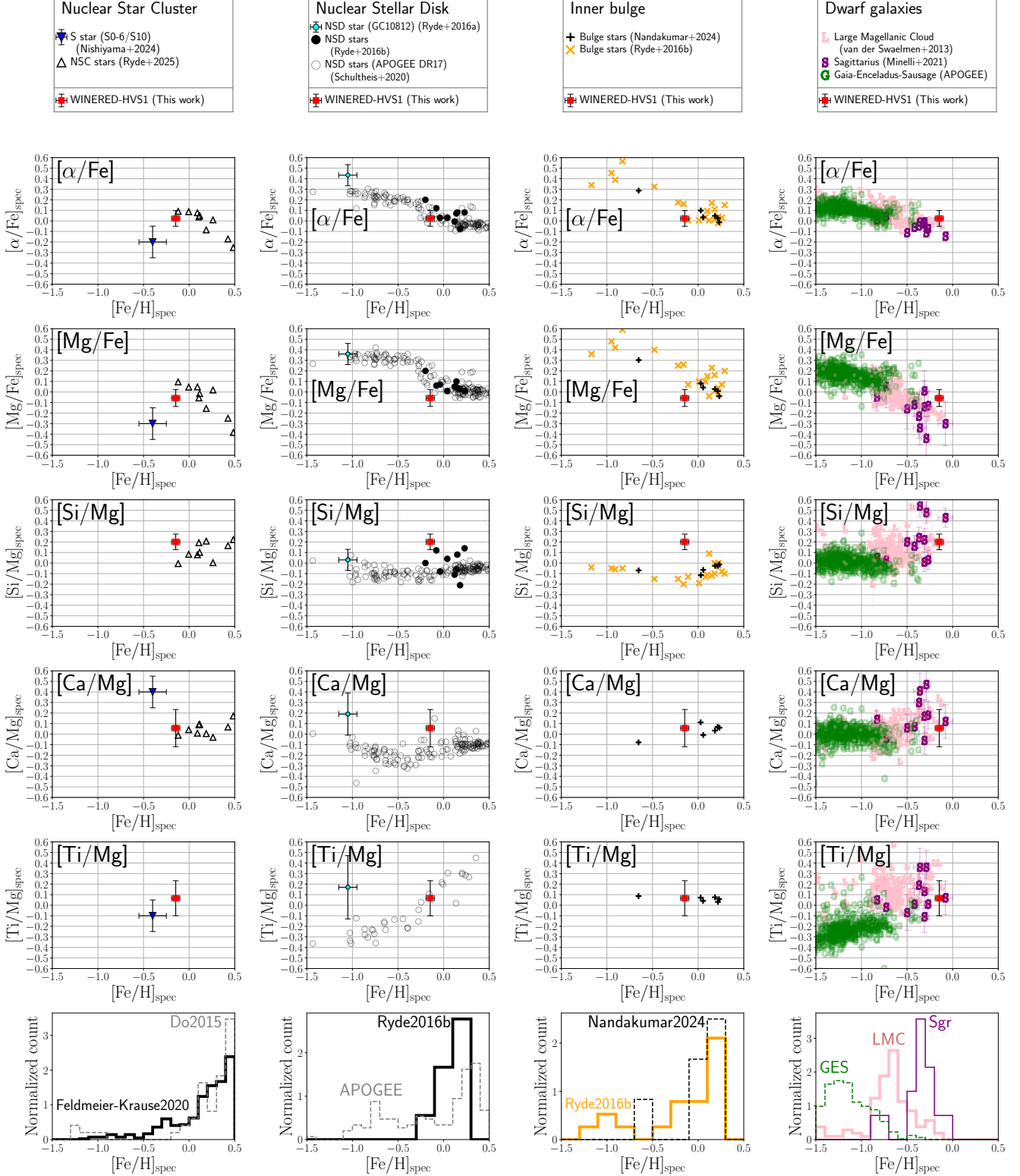


Figure 10. Chemistry of WINERED-HVS1 compared with stars in the NSC (left column), NSD (second column), inner bulge (third column), and dwarf galaxies (fourth column). The metal-rich, low- $[Mg/Fe]$ and high- $[Si/Mg]$ nature of WINERED-HVS1 is most consistent with the NSC stars. Intriguingly, WINERED-HVS1 is chemically similar to the metal-rich stars in massive dwarf galaxies; and it might have formed in the core of massive dwarf galaxy that merged to the Milky Way.

of dust in that direction, which demands extensive telescope time, especially in the near-infrared K band. By searching for many more HVSSs and by characterizing their chemical abundances with optical spectra, we will open a new window into the Galactic center environment without being hindered by dust obscuration.

8. SUMMARY AND CONCLUSION

By using astrometric data from Gaia DR3, photometric distance from StarHorse catalog (Anders et al. 2022), and $([M/H]_{XP}, [\alpha/M]_{XP})$ from Hattori (2025), we searched for candidates of metal-rich HVSSs ejected from the Galactic center. After selecting stars with some quality cut, we searched for stars that are kinematically consistent with HVSSs ejected from the Galactic center, by using four different sets of assumptions on the Galactic potential and on the Solar position/velocity. We find 74 kinematically selected metal-rich HVS candidates that are robust against the different assumptions.

We further pruned the sample by using the chemical data to identify 22 metal-rich HVS candidates, all of which were red giants (see Fig. 1). Unlike the only unambiguous HVS, S5-HVS1 (Koposov et al. 2020), our candidates are gravitationally bound to the Milky Way, and their ejection velocities are 500–600 km s⁻¹ (see Table 2). Thus, chemical characterizations of these stars is essential for understanding their origins.

Among these 22 candidates, 9 HVS candidates (labeled as mrHVSspec1-9) have spectroscopic abundances derived from large surveys (APOGEE, GALAH, RAVE, and LAMOST; see Table 3). The remaining 13 HVS candidates (labeled as WINERED-HVS1 and mrHVSxp2-13) lack existing spectroscopic abundances, but have relatively reliable estimates of $([M/H]_{XP}, [\alpha/M]_{XP})$ from Gaia XP spectra (Hattori 2025) (see Table 3).

Based on the metallicity and α -abundance of these stars, we cannot ignore the possibility that 21 stars out of our 22 candidates may be non-HVSSs. Namely, these 21 stars might be part of either the metal-rich tail of the GES (which is the remnants of the ancient major merger; Helmi et al. 2018; Belokurov et al. 2018), or the metal-poor tail of the high- α disk (which may be so-called Splash stars kicked out of the pre-existing disk when GES merged to the ancient Milky Way; Bonaca et al. 2017; Belokurov et al. 2020). In contrast to these 21 stars, one candidate, WINERED-HVS1, has a near-solar value of $[M/H]_{XP}$, making it unlikely to be classified as either a GES star or a Splash star.

To investigate this star further, we conducted a follow-up observation with Magellan/WINERED (see Section 6). Through a careful analysis of its high-resolution spectrum in the near-infrared YJ bands, we determined the metallicity $[Fe/H]$ as well as the abundances for Na, Mg, Si, S, K, Ca, Ti, Cr, Ni, and Sr (see Table 4). We obtained the metallicity and α -abundance $([Fe/H] = -0.147^{+0.046}_{-0.045}, [Mg/Fe] = -0.058^{+0.077}_{-0.082})$, which are consistent with $([M/H]_{XP}, [\alpha/M]_{XP})$.

Since WINERED-HVS1 has a bound orbit and it is not necessarily young, there is a possibility that this star was ejected from the (outer) Galactic disk. However, the observed value of $[Si/Mg]$ determined from our follow-up observations is distinct from that of Galactic disk stars, making this scenario unlikely (see Fig. 8). This analysis supports our view that the star was ejected from the Galactic center. Indeed, through Monte Carlo simulations (see Appendix E), we find that the ejection of WINERED-HVS1 with a velocity of $v_{ej} = 500$ – 600 km s⁻¹ via Hills mechanism involving the SMBH (Sgr A*) is dynamically viable.

To better understand the origin of this star, we compared the chemical properties of WINERED-HVS1 with those of other stars in the Milky Way and beyond (see Fig. 10). We found that WINERED-HVS1 is chemically consistent with stars in the NSC, but somewhat inconsistent with stars in the NSD or inner bulge, mainly due to its high $[Si/Mg]$ ratio. This result is promising, as HVSSs are ejected from the central region of the NSC, where the SMBH resides. Though the metallicity of WINERED-HVS1 is lower than that of typical NSC stars, it remains consistent with the metal-poor tail of NSC stars.

Another interesting point regarding the chemistry of WINERED-HVS1 is that the chemical abundance pattern of WINERED-HVS1 resembles the abundance pattern of the metal-rich stars in massive dwarf galaxies, such as the LMC or the Sagittarius dwarf galaxy. We do not think that WINERED-HVS1 was formed in either of these dwarf galaxies, because bringing this star to the central part of the Milky Way is unrealistic from a dynamical point of view. However, this chemical similarity indicates that this star may have formed in an environment similar to the core of a massive dwarf galaxy. Further observational studies are awaited to better understand the birth environment of this star.

The authors thank the anonymous referee for thorough reading and constructive comments. K.H. thanks Sergey E. Koposov for the inspiring collaboration at CMU, which provided valuable insights. Some of the insights gained during that time form a foundation for this work. K.H. is supported by JSPS KAKENHI Grant Numbers JP24K07101, JP21K13965, and JP21H00053. D.T. acknowledges financial support by the JSPS Research Fellowship for Young Scientists and the accompanying JSPS KAKENHI Grant Number 23KJ2149. T.T. acknowledges the support by JSPS KAKENHI Grant No. 23H00132.

This paper uses the WINERED data gathered with the 6.5 meter Magellan Telescope located at Las Campanas Observatory, Chile. We are grateful to Yuki Sarugaku, Tomomi Takeuchi, and the staff of Las Campanas Observatory for their support during the WINERED's observations. WINERED was developed by the University of Tokyo and the Laboratory of Infrared High-

resolution Spectroscopy, Kyoto Sangyo University, under the financial support of KAKENHI (Nos. 16684001, 20340042, and 21840052) and the MEXT Supported Program for the Strategic Research Foundation at Private Universities (Nos. S0801061 and S1411028). The observing run in 2023 June was partly supported by KAKENHI (grant No. 19KK0080) and JSPS Bilateral Program Number JPJSBP120239909.

This work has made use of data from the European Space Agency (ESA) mission *Gaia* (<https://www.cosmos.esa.int/gaia>), processed by the *Gaia* Data Processing and Analysis Consortium (DPAC, <https://www.cosmos.esa.int/web/gaia/dpac/consortium>). Funding

for the DPAC has been provided by national institutions, in particular the institutions participating in the *Gaia* Multilateral Agreement.

Facility: Magellan/WINERED, Gaia

Software: Agama (Vasiliev 2019), ATLAS9-APOGEE (Mészáros et al. 2012), BaSTI (Pietrinferni et al. 2004; Hidalgo et al. 2018), MOOG (Snedden 1973; Sneden et al. 2012), *mwDust* (Bovy et al. 2016), OCTOMAN (Taniguchi et al. 2025), SAGA (Suda et al. 2008), WARP (Hamano et al. 2024), matplotlib (Hunter 2007), numpy (van der Walt et al. 2011), scipy (Virtanen et al. 2020)

REFERENCES

- Abdurro'uf, Accetta, K., Aerts, C., et al. 2022, *ApJS*, 259, 35, doi: [10.3847/1538-4365/ac4414](https://doi.org/10.3847/1538-4365/ac4414)
- Akiba, T., Naoz, S., & Madigan, A.-M. 2024, arXiv e-prints, arXiv:2410.19881, doi: [10.48550/arXiv.2410.19881](https://doi.org/10.48550/arXiv.2410.19881)
- Alfaro-Cuello, M., Kacharov, N., Neumayer, N., et al. 2019, *ApJ*, 886, 57, doi: [10.3847/1538-4357/ab1b2c](https://doi.org/10.3847/1538-4357/ab1b2c)
- Anders, F., Khalatyan, A., Queiroz, A. B. A., et al. 2022, *A&A*, 658, A91, doi: [10.1051/0004-6361/202142369](https://doi.org/10.1051/0004-6361/202142369)
- Andrae, R., Rix, H.-W., & Chandra, V. 2023a, *ApJS*, 267, 8, doi: [10.3847/1538-4365/acd53e](https://doi.org/10.3847/1538-4365/acd53e)
- Andrae, R., Fouesneau, M., Sordo, R., et al. 2023b, *A&A*, 674, A27, doi: [10.1051/0004-6361/202243462](https://doi.org/10.1051/0004-6361/202243462)
- Andreasen, D. T., Sousa, S. G., Delgado Mena, E., et al. 2016, *A&A*, 585, A143, doi: [10.1051/0004-6361/201527308](https://doi.org/10.1051/0004-6361/201527308)
- Arca Sedda, M., Gualandris, A., Do, T., et al. 2020, *ApJL*, 901, L29, doi: [10.3847/2041-8213/abb245](https://doi.org/10.3847/2041-8213/abb245)
- Barbuy, B., Friça, A. C. S., Ernandes, H., et al. 2023, *MNRAS*, 526, 2365, doi: [10.1093/mnras/stad2888](https://doi.org/10.1093/mnras/stad2888)
- Belokurov, V., Erkal, D., Evans, N. W., Koposov, S. E., & Deason, A. J. 2018, *MNRAS*, 478, 611, doi: [10.1093/mnras/sty982](https://doi.org/10.1093/mnras/sty982)
- Belokurov, V., Sanders, J. L., Fattahi, A., et al. 2020, *MNRAS*, 494, 3880, doi: [10.1093/mnras/staa876](https://doi.org/10.1093/mnras/staa876)
- Bennett, M., & Bovy, J. 2019, *MNRAS*, 482, 1417, doi: [10.1093/mnras/sty2813](https://doi.org/10.1093/mnras/sty2813)
- Bland-Hawthorn, J., & Gerhard, O. 2016, *ARA&A*, 54, 529, doi: [10.1146/annurev-astro-081915-023441](https://doi.org/10.1146/annurev-astro-081915-023441)
- Bonaca, A., Conroy, C., Wetzell, A., Hopkins, P. F., & Kereš, D. 2017, *ApJ*, 845, 101, doi: [10.3847/1538-4357/aa7d0c](https://doi.org/10.3847/1538-4357/aa7d0c)
- Bovy, J., Rix, H.-W., Green, G. M., Schlafly, E. F., & Finkbeiner, D. P. 2016, *ApJ*, 818, 130, doi: [10.3847/0004-637X/818/2/130](https://doi.org/10.3847/0004-637X/818/2/130)
- Bressan, A., Marigo, P., Girardi, L., et al. 2012, *MNRAS*, 427, 127, doi: [10.1111/j.1365-2966.2012.21948.x](https://doi.org/10.1111/j.1365-2966.2012.21948.x)
- Bromley, B. C., Kenyon, S. J., Geller, M. J., et al. 2006, *ApJ*, 653, 1194, doi: [10.1086/508419](https://doi.org/10.1086/508419)
- Brown, W. R. 2015, *ARA&A*, 53, 15, doi: [10.1146/annurev-astro-082214-122230](https://doi.org/10.1146/annurev-astro-082214-122230)
- Brown, W. R., Geller, M. J., Kenyon, S. J., & Kurtz, M. J. 2005, *ApJL*, 622, L33, doi: [10.1086/429378](https://doi.org/10.1086/429378)
- Buder, S., Kos, J., Wang, E. X., et al. 2024, arXiv e-prints, arXiv:2409.19858, doi: [10.48550/arXiv.2409.19858](https://doi.org/10.48550/arXiv.2409.19858)
- Carr, J. S., Sellgren, K., & Balachandran, S. C. 2000, *ApJ*, 530, 307, doi: [10.1086/308340](https://doi.org/10.1086/308340)
- Chen, Y., Bressan, A., Girardi, L., et al. 2015, *MNRAS*, 452, 1068, doi: [10.1093/mnras/stv1281](https://doi.org/10.1093/mnras/stv1281)
- Clementini, G., Ripepi, V., Garofalo, A., et al. 2023, *A&A*, 674, A18, doi: [10.1051/0004-6361/202243964](https://doi.org/10.1051/0004-6361/202243964)
- Cunha, K., Sellgren, K., Smith, V. V., et al. 2007, *ApJ*, 669, 1011, doi: [10.1086/521813](https://doi.org/10.1086/521813)
- Cutri, R. M., Skrutskie, M. F., van Dyk, S., et al. 2003, 2MASS All Sky Catalog of point sources.
- Das, P., Hawkins, K., & Jofré, P. 2020, *MNRAS*, 493, 5195, doi: [10.1093/mnras/stz3537](https://doi.org/10.1093/mnras/stz3537)
- Davies, B., Origlia, L., Kudritzki, R.-P., et al. 2009, *ApJ*, 694, 46, doi: [10.1088/0004-637X/694/1/46](https://doi.org/10.1088/0004-637X/694/1/46)
- De Angeli, F., Weiler, M., Montegriffo, P., et al. 2023, *A&A*, 674, A2, doi: [10.1051/0004-6361/202243680](https://doi.org/10.1051/0004-6361/202243680)
- de Jong, R. S., Agertz, O., Berbel, A. A., et al. 2019, *The Messenger*, 175, 3, doi: [10.18727/0722-6691/5117](https://doi.org/10.18727/0722-6691/5117)
- Deason, A. J., Belokurov, V., & Sanders, J. L. 2019, *MNRAS*, 490, 3426, doi: [10.1093/mnras/stz2793](https://doi.org/10.1093/mnras/stz2793)
- Do, T., Kerzendorf, W., Winsor, N., et al. 2015, *ApJ*, 809, 143, doi: [10.1088/0004-637X/809/2/143](https://doi.org/10.1088/0004-637X/809/2/143)
- Drimmel, R., Cabrera-Lavers, A., & López-Corredoira, M. 2003, *A&A*, 409, 205, doi: [10.1051/0004-6361:20031070](https://doi.org/10.1051/0004-6361:20031070)
- Ernandes, H., Feuillet, D., Feltzing, S., & Skúladóttir, Á. 2024, *A&A*, 691, A333, doi: [10.1051/0004-6361/202450827](https://doi.org/10.1051/0004-6361/202450827)

- Feldmeier-Krause, A. 2022, MNRAS, 513, 5920, doi: [10.1093/mnras/stac1227](https://doi.org/10.1093/mnras/stac1227)
- Feldmeier-Krause, A., Kerzendorf, W., Do, T., et al. 2020, MNRAS, 494, 396, doi: [10.1093/mnras/staa703](https://doi.org/10.1093/mnras/staa703)
- Feuillet, D. K., Feltzing, S., Sahlholdt, C., & Bensby, T. 2022, ApJ, 934, 21, doi: [10.3847/1538-4357/ac76ba](https://doi.org/10.3847/1538-4357/ac76ba)
- Feuillet, D. K., Sahlholdt, C. L., Feltzing, S., & Casagrande, L. 2021, MNRAS, 508, 1489, doi: [10.1093/mnras/stab2614](https://doi.org/10.1093/mnras/stab2614)
- Fouesneau, M., Frémat, Y., Andrae, R., et al. 2023, A&A, 674, A28, doi: [10.1051/0004-6361/202243919](https://doi.org/10.1051/0004-6361/202243919)
- Fukue, K., Matsunaga, N., Kondo, S., et al. 2021, ApJ, 913, 62, doi: [10.3847/1538-4357/abf0b1](https://doi.org/10.3847/1538-4357/abf0b1)
- Gaia Collaboration, Prusti, T., de Bruijne, J. H. J., et al. 2016, A&A, 595, A1, doi: [10.1051/0004-6361/201629272](https://doi.org/10.1051/0004-6361/201629272)
- Gaia Collaboration, Brown, A. G. A., Vallenari, A., et al. 2018, A&A, 616, A1, doi: [10.1051/0004-6361/201833051](https://doi.org/10.1051/0004-6361/201833051)
- . 2021, A&A, 649, A1, doi: [10.1051/0004-6361/202039657](https://doi.org/10.1051/0004-6361/202039657)
- Gaia Collaboration, Vallenari, A., Brown, A. G. A., et al. 2023, A&A, 674, A1, doi: [10.1051/0004-6361/202243940](https://doi.org/10.1051/0004-6361/202243940)
- Ghez, A. M., Duchêne, G., Matthews, K., et al. 2003, ApJL, 586, L127, doi: [10.1086/374804](https://doi.org/10.1086/374804)
- Gillessen, S., Plewa, P. M., Eisenhauer, F., et al. 2017, ApJ, 837, 30, doi: [10.3847/1538-4357/aa5c41](https://doi.org/10.3847/1538-4357/aa5c41)
- GRAVITY Collaboration, Abuter, R., Aymar, N., et al. 2022, A&A, 657, L12, doi: [10.1051/0004-6361/202142465](https://doi.org/10.1051/0004-6361/202142465)
- Green, G. M., Schlafly, E., Zucker, C., Speagle, J. S., & Finkbeiner, D. 2019, ApJ, 887, 93, doi: [10.3847/1538-4357/ab5362](https://doi.org/10.3847/1538-4357/ab5362)
- Guillard, N., Emsellem, E., & Renaud, F. 2016, MNRAS, 461, 3620, doi: [10.1093/mnras/stw1570](https://doi.org/10.1093/mnras/stw1570)
- Hamano, S., Ikeda, Y., Otsubo, S., et al. 2024, PASP, 136, 014504, doi: [10.1088/1538-3873/ad1b38](https://doi.org/10.1088/1538-3873/ad1b38)
- Hattori, K. 2025, ApJ, 980, 90, doi: [10.3847/1538-4357/ad9686](https://doi.org/10.3847/1538-4357/ad9686)
- Hattori, K., Okuno, A., & Roederer, I. U. 2023, ApJ, 946, 48, doi: [10.3847/1538-4357/acb93b](https://doi.org/10.3847/1538-4357/acb93b)
- Hattori, K., Valluri, M., Bell, E. F., & Roederer, I. U. 2018a, ApJ, 866, 121, doi: [10.3847/1538-4357/aadee5](https://doi.org/10.3847/1538-4357/aadee5)
- Hattori, K., Valluri, M., & Castro, N. 2018b, ApJ, 869, 33, doi: [10.3847/1538-4357/aaed22](https://doi.org/10.3847/1538-4357/aaed22)
- Hattori, K., Valluri, M., Castro, N., et al. 2019, ApJ, 873, 116, doi: [10.3847/1538-4357/ab05c8](https://doi.org/10.3847/1538-4357/ab05c8)
- Helmi, A., Babusiaux, C., Koppelman, H. H., et al. 2018, Nature, 563, 85, doi: [10.1038/s41586-018-0625-x](https://doi.org/10.1038/s41586-018-0625-x)
- Hidalgo, S. L., Pietrinferni, A., Cassisi, S., et al. 2018, ApJ, 856, 125, doi: [10.3847/1538-4357/aab158](https://doi.org/10.3847/1538-4357/aab158)
- Hills, J. G. 1988, Nature, 331, 687, doi: [10.1038/331687a0](https://doi.org/10.1038/331687a0)
- Horta, D., Schiavon, R. P., Mackereth, J. T., et al. 2021, MNRAS, 500, 1385, doi: [10.1093/mnras/staa2987](https://doi.org/10.1093/mnras/staa2987)
- . 2023, MNRAS, 520, 5671, doi: [10.1093/mnras/stac3179](https://doi.org/10.1093/mnras/stac3179)
- Hunter, J. D. 2007, Computing in Science and Engineering, 9, 90, doi: [10.1109/MCSE.2007.55](https://doi.org/10.1109/MCSE.2007.55)
- Ikeda, Y., Kondo, S., Otsubo, S., et al. 2022, PASP, 134, 015004, doi: [10.1088/1538-3873/ac1c5f](https://doi.org/10.1088/1538-3873/ac1c5f)
- Jin, S., Trager, S. C., Dalton, G. B., et al. 2023, MNRAS, doi: [10.1093/mnras/stad557](https://doi.org/10.1093/mnras/stad557)
- Jofré, E., Petrucci, R., Saffe, C., et al. 2015, A&A, 574, A50, doi: [10.1051/0004-6361/201424474](https://doi.org/10.1051/0004-6361/201424474)
- Jofré, P., Heiter, U., & Soubiran, C. 2019, ARA&A, 57, 571, doi: [10.1146/annurev-astro-091918-104509](https://doi.org/10.1146/annurev-astro-091918-104509)
- Jofré, P., Heiter, U., Tucci Maia, M., et al. 2018, Research Notes of the American Astronomical Society, 2, 152, doi: [10.3847/2515-5172/aadc61](https://doi.org/10.3847/2515-5172/aadc61)
- Kondo, S., Fukue, K., Matsunaga, N., et al. 2019, ApJ, 875, 129, doi: [10.3847/1538-4357/ab0ec4](https://doi.org/10.3847/1538-4357/ab0ec4)
- Koposov, S. E., Boubert, D., Li, T. S., et al. 2020, MNRAS, 491, 2465, doi: [10.1093/mnras/stz3081](https://doi.org/10.1093/mnras/stz3081)
- Kruijssen, J. M. D., Pfeffer, J. L., Reina-Campos, M., Crain, R. A., & Bastian, N. 2019, MNRAS, 486, 3180, doi: [10.1093/mnras/sty1609](https://doi.org/10.1093/mnras/sty1609)
- Leonard, P. J. T. 1991, AJ, 101, 562, doi: [10.1086/115704](https://doi.org/10.1086/115704)
- Levin, Y. 2007, MNRAS, 374, 515, doi: [10.1111/j.1365-2966.2006.11155.x](https://doi.org/10.1111/j.1365-2966.2006.11155.x)
- Li, Y.-B., Luo, A. L., Lu, Y.-J., et al. 2021, ApJS, 252, 3, doi: [10.3847/1538-4365/abc16e](https://doi.org/10.3847/1538-4365/abc16e)
- Marchetti, T. 2021, MNRAS, 503, 1374, doi: [10.1093/mnras/stab599](https://doi.org/10.1093/mnras/stab599)
- Marchetti, T., Contigiani, O., Rossi, E. M., et al. 2018, MNRAS, 476, 4697, doi: [10.1093/mnras/sty579](https://doi.org/10.1093/mnras/sty579)
- Marchetti, T., Evans, F. A., & Rossi, E. M. 2022, MNRAS, 515, 767, doi: [10.1093/mnras/stac1777](https://doi.org/10.1093/mnras/stac1777)
- Marchetti, T., Rossi, E. M., & Brown, A. G. A. 2019, MNRAS, 490, 157, doi: [10.1093/mnras/sty2592](https://doi.org/10.1093/mnras/sty2592)
- Marshall, D. J., Robin, A. C., Reylé, C., Schultheis, M., & Picaud, S. 2006, A&A, 453, 635, doi: [10.1051/0004-6361:20053842](https://doi.org/10.1051/0004-6361:20053842)
- Matsunaga, N., Taniguchi, D., Jian, M., et al. 2020, ApJS, 246, 10, doi: [10.3847/1538-4365/ab5c25](https://doi.org/10.3847/1538-4365/ab5c25)
- McMillan, P. J. 2017, MNRAS, 465, 76, doi: [10.1093/mnras/stw2759](https://doi.org/10.1093/mnras/stw2759)
- Meléndez, J., & Barbuy, B. 1999, ApJS, 124, 527, doi: [10.1086/313261](https://doi.org/10.1086/313261)
- Mészáros, S., Allende Prieto, C., Edvardsson, B., et al. 2012, AJ, 144, 120, doi: [10.1088/0004-6256/144/4/120](https://doi.org/10.1088/0004-6256/144/4/120)
- Minelli, A., Mucciarelli, A., Romano, D., et al. 2021, ApJ, 910, 114, doi: [10.3847/1538-4357/abe3f9](https://doi.org/10.3847/1538-4357/abe3f9)
- Montegriffo, P., De Angeli, F., Andrae, R., et al. 2023, A&A, 674, A3, doi: [10.1051/0004-6361/202243880](https://doi.org/10.1051/0004-6361/202243880)

- Nandakumar, G., Ryde, N., Schultheis, M., et al. 2025, *ApJL*, 982, L14, doi: [10.3847/2041-8213/adbb6d](https://doi.org/10.3847/2041-8213/adbb6d)
- Nandakumar, G., Ryde, N., Mace, G., et al. 2024, *ApJ*, 964, 96, doi: [10.3847/1538-4357/ad22dc](https://doi.org/10.3847/1538-4357/ad22dc)
- Neumayer, N., Seth, A., & Böker, T. 2020, *A&A Rv*, 28, 4, doi: [10.1007/s00159-020-00125-0](https://doi.org/10.1007/s00159-020-00125-0)
- Nishiyama, S., Yasui, K., Nagata, T., et al. 2013, *ApJL*, 769, L28, doi: [10.1088/2041-8205/769/2/L28](https://doi.org/10.1088/2041-8205/769/2/L28)
- Nishiyama, S., Kara, T., Thorsbro, B., et al. 2024, *Proceedings of the Japan Academy, Series B*, 100, 86, doi: [10.2183/pjab.100.007](https://doi.org/10.2183/pjab.100.007)
- Okuno, A., & Hattori, K. 2022, arXiv e-prints, arXiv:2204.08205, doi: [10.48550/arXiv.2204.08205](https://doi.org/10.48550/arXiv.2204.08205)
- Perets, H. B., & Šubr, L. 2012, *ApJ*, 751, 133, doi: [10.1088/0004-637X/751/2/133](https://doi.org/10.1088/0004-637X/751/2/133)
- Pfuhl, O., Fritz, T. K., Zilka, M., et al. 2011, *ApJ*, 741, 108, doi: [10.1088/0004-637X/741/2/108](https://doi.org/10.1088/0004-637X/741/2/108)
- Pietrinferni, A., Cassisi, S., Salaris, M., & Castelli, F. 2004, *ApJ*, 612, 168, doi: [10.1086/422498](https://doi.org/10.1086/422498)
- Piffl, T., Binney, J., McMillan, P. J., et al. 2014, *MNRAS*, 445, 3133, doi: [10.1093/mnras/stu1948](https://doi.org/10.1093/mnras/stu1948)
- Pinsonneault, M. H., Zinn, J. C., Tayar, J., et al. 2025, *ApJS*, 276, 69, doi: [10.3847/1538-4365/ad9fef](https://doi.org/10.3847/1538-4365/ad9fef)
- Portail, M., Gerhard, O., Wegg, C., & Ness, M. 2017, *MNRAS*, 465, 1621, doi: [10.1093/mnras/stw2819](https://doi.org/10.1093/mnras/stw2819)
- Portegies Zwart, S. F., McMillan, S. L. W., & Gieles, M. 2010, *ARA&A*, 48, 431, doi: [10.1146/annurev-astro-081309-130834](https://doi.org/10.1146/annurev-astro-081309-130834)
- Ramírez, S. V., Sellgren, K., Carr, J. S., et al. 2000, *ApJ*, 537, 205, doi: [10.1086/309022](https://doi.org/10.1086/309022)
- Reid, M. J., & Brunthaler, A. 2020, *ApJ*, 892, 39, doi: [10.3847/1538-4357/ab76cd](https://doi.org/10.3847/1538-4357/ab76cd)
- Rich, R. M., Ryde, N., Thorsbro, B., et al. 2017, *AJ*, 154, 239, doi: [10.3847/1538-3881/aa970a](https://doi.org/10.3847/1538-3881/aa970a)
- Ryabchikova, T., Piskunov, N., Kurucz, R. L., et al. 2015, *PhyS*, 90, 054005, doi: [10.1088/0031-8949/90/5/054005](https://doi.org/10.1088/0031-8949/90/5/054005)
- Ryde, N., Fritz, T. K., Rich, R. M., et al. 2016a, *ApJ*, 831, 40, doi: [10.3847/0004-637X/831/1/40](https://doi.org/10.3847/0004-637X/831/1/40)
- Ryde, N., Schultheis, M., Grieco, V., et al. 2016b, *AJ*, 151, 1, doi: [10.3847/0004-6256/151/1/1](https://doi.org/10.3847/0004-6256/151/1/1)
- Ryde, N., Nandakumar, G., Schultheis, M., et al. 2025, *ApJ*, 979, 174, doi: [10.3847/1538-4357/ad9b2b](https://doi.org/10.3847/1538-4357/ad9b2b)
- Sameshima, H., Matsunaga, N., Kobayashi, N., et al. 2018, *PASP*, 130, 074502, doi: [10.1088/1538-3873/aac1b4](https://doi.org/10.1088/1538-3873/aac1b4)
- Schödel, R., Feldmeier, A., Neumayer, N., Meyer, L., & Yelda, S. 2014, *Classical and Quantum Gravity*, 31, 244007, doi: [10.1088/0264-9381/31/24/244007](https://doi.org/10.1088/0264-9381/31/24/244007)
- Schönrich, R., Binney, J., & Dehnen, W. 2010, *MNRAS*, 403, 1829, doi: [10.1111/j.1365-2966.2010.16253.x](https://doi.org/10.1111/j.1365-2966.2010.16253.x)
- Schultheis, M., Rojas-Arriagada, A., Cunha, K., et al. 2020, *A&A*, 642, A81, doi: [10.1051/0004-6361/202038327](https://doi.org/10.1051/0004-6361/202038327)
- Schultheis, M., Fritz, T. K., Nandakumar, G., et al. 2021, *A&A*, 650, A191, doi: [10.1051/0004-6361/202140499](https://doi.org/10.1051/0004-6361/202140499)
- Snedden, C. 1973, *ApJ*, 184, 839, doi: [10.1086/152374](https://doi.org/10.1086/152374)
- Snedden, C., Bean, J., Ivans, I., Lucatello, S., & Sobek, J. 2012, MOOG: LTE line analysis and spectrum synthesis, Astrophysics Source Code Library, record ascl:1202.009. <http://ascl.net/1202.009>
- Steinmetz, M., Guiglion, G., McMillan, P. J., et al. 2020, *AJ*, 160, 83, doi: [10.3847/1538-3881/ab9ab8](https://doi.org/10.3847/1538-3881/ab9ab8)
- Suda, T., Katsuta, Y., Yamada, S., et al. 2008, *PASJ*, 60, 1159, doi: [10.1093/pasj/60.5.1159](https://doi.org/10.1093/pasj/60.5.1159)
- Takada, M., Ellis, R. S., Chiba, M., et al. 2014, *PASJ*, 66, R1, doi: [10.1093/pasj/pst019](https://doi.org/10.1093/pasj/pst019)
- Taniguchi, D., Matsunaga, N., Kobayashi, N., et al. 2018, *MNRAS*, 473, 4993, doi: [10.1093/mnras/stx2691](https://doi.org/10.1093/mnras/stx2691)
- Taniguchi, D., Matsunaga, N., Jian, M., et al. 2021, *MNRAS*, 502, 4210, doi: [10.1093/mnras/staa3855](https://doi.org/10.1093/mnras/staa3855)
- Taniguchi, D., Matsunaga, N., Kobayashi, N., et al. 2025, *A&A*, 693, A163, doi: [10.1051/0004-6361/202452392](https://doi.org/10.1051/0004-6361/202452392)
- Tauris, T. M. 2015, *MNRAS*, 448, L6, doi: [10.1093/mnrasl/slu189](https://doi.org/10.1093/mnrasl/slu189)
- Van der Swaelmen, M., Hill, V., Primas, F., & Cole, A. A. 2013, *A&A*, 560, A44, doi: [10.1051/0004-6361/201321109](https://doi.org/10.1051/0004-6361/201321109)
- van der Walt, S., Colbert, S. C., & Varoquaux, G. 2011, *Computing in Science Engineering*, 13, 22, doi: [10.1109/MCSE.2011.37](https://doi.org/10.1109/MCSE.2011.37)
- Vasiliev, E. 2019, *MNRAS*, 482, 1525, doi: [10.1093/mnras/sty2672](https://doi.org/10.1093/mnras/sty2672)
- Verberne, S., Rossi, E. M., Kuposov, S. E., et al. 2024, *MNRAS*, 533, 2747, doi: [10.1093/mnras/stae1888](https://doi.org/10.1093/mnras/stae1888)
- Virtanen, P., Gommers, R., Oliphant, T. E., et al. 2020, *Nature Methods*, 17, 261, doi: [10.1038/s41592-019-0686-2](https://doi.org/10.1038/s41592-019-0686-2)
- Zhang, F., Lu, Y., & Yu, Q. 2013, *ApJ*, 768, 153, doi: [10.1088/0004-637X/768/2/153](https://doi.org/10.1088/0004-637X/768/2/153)
- Zhang, X., Green, G. M., & Rix, H.-W. 2023, *MNRAS*, 524, 1855, doi: [10.1093/mnras/stad1941](https://doi.org/10.1093/mnras/stad1941)
- Zhao, G., Zhao, Y., Chu, Y., Jing, Y., & Deng, L. 2012, arXiv e-prints, arXiv:1206.3569. <https://arxiv.org/abs/1206.3569>

APPENDIX

A. SPECTRAL ANALYSIS USING A DIFFERENT LINE LIST

In the main part of this paper, we use the MB99 line list (Meléndez & Barbuy 1999) to derive the chemical abundances of WINERED-HVS1. Table 5 shows the same result but using the VALD3 line list (Ryabchikova et al. 2015).

B. MASS AND AGE OF WINERED-HVS1 AND OTHER METAL-RICH HVS CANDIDATES

B.1. WINERED-HVS1

Given the location of WINERED-HVS1 in the CMD, it could be either a red clump star or a red giant branch star. If it is a red clump star, its mass can be $1\text{--}2M_{\odot}$, implying an old age. In contrast, if it is a red giant branch star, its mass can be $2\text{--}3M_{\odot}$, implying a younger age. We currently do not have enough data to determine whether this star is a red clump star or red giant branch star. Therefore, we estimate its stellar age using two ways, each based on the assumption that the star is in one of these two stages.

From the APOKASC-3 catalog (Pinsonneault et al. 2025), which provides reliable stellar ages from asteroseismology, we selected red giant branch stars and red clump stars whose astrophysical parameters are similar to those of WINERED-HVS1. In the following analysis, we used the effective temperature $T_{\text{eff}}^{\text{xgboost}}$, surface gravity $\log g^{\text{xgboost}}$, and metallicity $[M/H]^{\text{xgboost}}$ in Andrae et al. (2023a) estimated from Gaia XP spectra. First, by using the APOKASC-3 red giant branch sample, we estimated the relationship between $T_{\text{eff}}^{\text{xgboost}}$, $\log g^{\text{xgboost}}$, and stellar age. We then used this relationship as well as the values $(T_{\text{eff}}^{\text{xgboost}}/\text{K}, \log g^{\text{xgboost}}) = (4808.1, 2.416)$ of WINERED-HVS1 to estimate its age in a Bayesian manner. We find that the stellar age is 0.5–3 Gyr (95% range of the posterior distribution) if this star is a red giant branch star. Secondly, we repeated the same analysis by using the APOKASC-3 red clump star sample. In this case, we find that the stellar age is 2–10 Gyr (95% range) if this star is a red clump star. Since we are not sure whether this star is a red giant branch or red clump star, we conclude that its age is likely 0.5–10 Gyr. Finally, by comparing $[M/H]^{\text{xgboost}}$, the evolutionary stage (i.e., red giant), and the estimated age of this star with the predictions from the PARSEC isochrone models version 1.2S (Bressan et al. 2012; Chen et al. 2015), we estimate its mass to be $1\text{--}3M_{\odot}$.

We note that Gaia DR3 estimated its age to be `age_flame`=0.4–0.7 Gyr and its mass to be `mass_flame`=2.4–2.9 M_{\odot} . However, their estimates should be treated with caution. As described in Fouesneau et al. (2023), when they estimated the stellar parameters by comparing the data and theoretical isochrone models, they only considered the stellar evolution stages from the zero-age-main-sequence to the tip of the giant branch, and they did not consider the possibility of the red clump stage. Indeed, their age estimate (0.4–0.7 Gyr) is consistent with our estimate of 0.5–3 Gyr, under the assumption that it is a red giant branch star. We also note that StarHorse catalog (v1.2) estimated its mass to be 0.86–0.95 M_{\odot} , which is consistent with the interpretation that this star is a red clump star.

B.2. Other metal-rich HVS candidates

For the other metal-rich HVSs candidates, we roughly estimated their stellar masses to be $1\text{--}3M_{\odot}$ based on the CMD, although we did not analyze these stars as thoroughly as WINERED-HVS1.

C. SELECTION OF NEARLY RADIAL ORBIT STARS IN APOGEE AND GAIA XP SAMPLES

In Fig. 6, we show the stars with nearly radial orbits in APOGEE sample and in Gaia XP sample. This APOGEE sample is also used to represent the GES stars in Fig. 10. Here we describe how these samples are selected.

For APOGEE DR17 sample, we first select stars that satisfy: `SNR`> 80, `TEFF`< 6000, `LOGG`< 3.5, `FE_H`> -1 , `MG_FE`> -0.5 , `SI_FE`> -0.5 , `CA_FE`> -0.5 , `TI_FE`> -0.5 , `MG_FE_ERR`< 0.05, `STARFLAG` is 0, `ASPCAPFLAG` is 0, `MEMBERFLAG` is 0, `PROGRAMNAME` is not ‘magclouds’ (removing Magellanic Clouds regions), 22nd and 23rd bits of `APOGEE2_TARGET1` is 0 (removing potential member stars of Sagittarius dwarf galaxy or LMC), and 4th bit of `EXTRATARG` is 0 (removing duplicate observations).

For Gaia XP sample, we first select stars from the catalog of Hattori (2025) that satisfy: `bool_flag_cmd_good`=True, `mh_50_qrf`> -1 , `mh_84_qrf`–`mh_16_qrf`< 0.5, `alpham_84_qrf`–`alpham_16_qrf`< 0.16, `G`< 13, and `RUWE`< 1.4.

After these selections, for both APOGEE DR17 sample and Gaia XP sample, we select stars with good parallax (`parallax_over_error`> 5). We compute the stellar position and velocity as in Section 3.1. We select stars with bound orbit, and compute the radial and azimuthal orbital action J_r and J_{ϕ} . Finally, we select stars with radial orbits by imposing $30 < (J_r/(\text{kpc km s}^{-1}))^{1/2} < 55$ and $|J_{\phi}| < 500 \text{ kpc km s}^{-1}$, following Feuillet et al. (2021).

D. SELECTION OF DISK STARS IN APOGEE SAMPLE

The disk stars in Fig. 8 are selected in the following manner. First, from the APOGEE DR17 catalog, we select stars with: `SNR`> 80, `TEFF`< 6000, `LOGG`< 3.5, `FE_H`> -1 , `MG_FE`> -0.5 , `SI_FE`> -0.5 , `FE_H_ERR`< 0.1,

Table 5. Chemical abundances of WINERED-HVS1 measured with the VALD3 line list (Ryabchikova et al. 2015)

v_{micro} [km s ⁻¹]	1.453 ^{+0.188} _{-0.186}	
[Fe/H] [dex]	-0.162 ^{+0.051} _{-0.047} (46)	
	[X/H] [dex]	[X/Fe] [dex]
Na I	—	—
Mg I	-0.146 ^{+0.127} _{-0.126}	+0.016 ^{+0.140} _{-0.144} (2)
Si I	+0.007 ^{+0.085} _{-0.080}	+0.169 ^{+0.088} _{-0.091} (19)
S I	+0.081 ^{+0.278} _{-0.262}	+0.243 ^{+0.274} _{-0.267} (1)
K I	—	—
Ca I	-0.042 ^{+0.156} _{-0.156}	+0.120 ^{+0.162} _{-0.165} (7)
Ti I	-0.155 ^{+0.142} _{-0.145}	+0.007 ^{+0.140} _{-0.153} (11)
Cr I	-0.157 ^{+0.135} _{-0.134}	+0.005 ^{+0.138} _{-0.143} (9)
Ni I	-0.059 ^{+0.137} _{-0.134}	+0.103 ^{+0.137} _{-0.137} (2)
Sr II	+0.120 ^{+0.236} _{-0.229}	+0.282 ^{+0.236} _{-0.233} (1)

MG_FE_ERR < 0.05, SI_FE_ERR < 0.05, STARFLAG is 0, ASPCAPFLAG is 0, MEMBERFLAG is 0, PROGRAM-NAME is not ‘magclouds’, 22nd and 23rd bits of APOGEE2_TARGET1 is 0, and 4th bit of EXTRATARG is 0. We then select stars with good parallax from Gaia DR3 (parallax_over_error > 5). Finally, we compute the Galactocentric position of the stars as in Section 3.1 and select stars at $|z| < 0.5$ kpc from the disk plane.

E. MONTE CARLO SIMULATIONS OF HYPER-VELOCITY STARS

E.1. Empirical model of Hills mechanism

According to the theoretical investigations by Hills (1988) and Bromley et al. (2006), the typical ejection velocity of an HVS due to the Hills mechanism—involving the 3-body interaction between a SMBH (with mass M_{BH}) and a stellar binary (consisting of two stars separated by a semi-major axis a with masses of m_1 and m_2)—is given by:

$$v_{\text{ej}} = 1370 \text{ km s}^{-1} \left(\frac{a}{0.1 \text{ AU}} \right)^{-1/2} \left(\frac{m_1 + m_2}{M_{\odot}} \right)^{1/2} \left(\frac{M_{\text{BH}}}{4 \times 10^6 M_{\odot}} \right)^{1/6} f_R. \quad (\text{E1})$$

In this equation, v_{ej} represents the typical velocity of the escaping star once it has left the gravitational influence of the SMBH (at a distance of ~ 1 pc from the SMBH). In the main part of this paper, we employ two models of the Galactic gravitational potential that do not account for the SMBH’s potential. Therefore, the ejection velocity v_{ej} computed in the main text for stars in the Gaia catalog can be directly compared with the value of v_{ej} provided in equation (E1).

We note that the empirical factor $f_R < 1$ is of order unity and depends on the dimensionless quantity

$$D = \frac{r_{\text{peri}}}{a} \left(\frac{10^6 M_{\odot} m_1 + m_2}{M_{\text{BH}} 2M_{\odot}} \right)^{1/3}. \quad (\text{E2})$$

In this equation, r_{peri} represents the closest approach distance between the binary system and the SMBH. The approximate formula for $f_R(D)$ provided by Bromley et al. (2006) is

$$f_R(D) = \sum_{k=0}^5 c_k D^k \quad (\text{for } 0 \leq D \leq 175) \quad (\text{E3})$$

with coefficients given by $(c_0, c_1, c_2, c_3, c_4, c_5) = (0.774, 0.0204, -6.23 \times 10^{-4}, 7.62 \times 10^{-6}, -4.24 \times 10^{-8}, 8.62 \times 10^{-11})$. The quantity D also governs the empirical ejection probability, which can be expressed as

$$P_{\text{ej}} = \begin{cases} 1 - \frac{D}{175} & (\text{for } 0 \leq D \leq 175), \\ 0 & (\text{otherwise}). \end{cases} \quad (\text{E4})$$

E.2. Simulations of HVS ejections

In the main analysis of this paper, we find that WINERED-HVS1 and other metal-rich HVS candidates have ejection velocities of 500–600 km s⁻¹. These stars have stellar masses of around 1–3M_⊙ (see Appendix B). To understand the physical parameters that lead to the ejection of a 1–3M_⊙ star with an ejection velocity ranging from 500 to 600 km s⁻¹, we perform Monte Carlo simulations consisting of $n_{\text{MC}} = 5 \times 10^5$ realizations. In the following analysis, we assume that $M_{\text{BH}} = 4 \times 10^6 M_{\odot}$. In Appendix E.2.1, we assume $m_1 = m_2 = 3M_{\odot}$. In Appendix E.2.2, we also perform similar simulations assuming $m_1 = m_2 = 2M_{\odot}$ or $m_1 = m_2 = 1M_{\odot}$.

E.2.1. A Monte Carlo simulation of 3-M_⊙ HVSs

Following Bromley et al. (2006), we assume that the binary’s closest approach to the SMBH satisfies the condition 1 AU < r_{peri} < 700 AU. To simplify our calculations, we assume that r_{peri} is equal to the impact parameter of the center-of-mass orbit of the binary at infinity. In this context, the probability of having the impact parameter between r_{peri} and $r_{\text{peri}} + dr_{\text{peri}}$ is proportional to $2\pi r_{\text{peri}} dr_{\text{peri}}$. We randomly sample n_{MC} values of r_{peri} from the range 1 AU < r_{peri} < 700 AU according to this probability distribution.

Additionally, following Bromley et al. (2006), we assume that the logarithmic value of the binary’s semi-major axis, $\ln a$, follows a uniform distribution. The lower limit for a is set at $a_{\text{min}} = 0.028$ AU, which is the minimum allowed value of a so that two 3-M_⊙ main-sequence stars in a binary do not merge.¹⁹ (Due to the assumption in a_{min} , our simulation technically addresses the ejection of 3-M_⊙ main-sequence HVSs. However, this simulation can be also used to gain insights into the ejection of 3-M_⊙ red giant HVSs, as we will demonstrate later.) The upper limit for a is set at 100 AU, which is sufficiently large that our analysis is not sensitive to this value. We also randomly sample n_{MC} values of a according to this probability distribution.

For each pair (a, r_{peri}) , we calculate three quantities: D , the ejection velocity v_{ej} , and the ejection probability P_{ej} . If P_{ej} is non-zero, we store the corresponding v_{ej} with a probability of P_{ej} . Out of $n_{\text{MC}} = 5 \times 10^5$ realizations, we find that 2457 realizations result in an ejection with $v_{\text{ej}} = 500$ –600 km s⁻¹. The fraction of ejections within this range of v_{ej} is small, mainly because the upper limit for a is set very high. Under our current assumptions, no HVSs would be ejected with $v_{\text{ej}} > 500$ km s⁻¹ if $a > 5$ AU is satisfied.

Fig. 11(a)–(c) illustrates the results of this analysis. For an HVS with a mass of 3M_⊙, achieving an ejection velocity of 500–600 km s⁻¹ typically requires $a \sim 3.1$ AU (median) and $r_{\text{peri}} \simeq 230$ AU (median). The values of a and r_{peri} can vary by a factor of around 2. Our result indicates that a binary system consisting of two 3-M_⊙ main-sequence stars can interact with the Galactic SMBH to produce a main-sequence HVS with an ejection velocity of 500–600 km s⁻¹.

While this simulation focuses on the ejection of main-sequence HVSs, our simulation can also provide insights into the ejection of red giant HVSs of similar masses. For $a > 0.526$ AU, the Roche radius of an equal-mass binary satisfies $R_{\text{Roche}} = 0.38a > 0.2$ AU. Given that a 3-M_⊙ red giant star typically has a radius smaller than 0.2 AU, a condition of $a > 0.526$ AU is a sufficient condition for a binary system consisting of two 3-M_⊙ red giants does not merge. In this regard, it is noteworthy that all the Monte Carlo realizations that yielded $v_{\text{ej}} = 500$ –600 km s⁻¹ satisfy the condition $a > 0.526$ AU. Our result indicates that a binary system consisting of two 3-M_⊙ red giant stars can interact with the Galactic SMBH to produce a red-giant HVS with an ejection velocity of 500–600 km s⁻¹.

E.2.2. Monte Carlo simulations of 2-M_⊙ HVSs and 1-M_⊙ HVSs

We conduct the same Monte Carlo simulation but assuming $m_1 = m_2 = 2M_{\odot}$ and $a_{\text{min}} = 0.026$ AU; or $m_1 = m_2 = 1M_{\odot}$ and $a_{\text{min}} = 0.012$ AU. Here, a_{min} is set by the same requirement as in Appendix E.2.1. Figs. 11(d)–(f) and (g)–(i) illustrate the results of these analyses. By using the fact that 2-M_⊙ (1-M_⊙) red giant stars typically have a radius smaller than 0.2 AU (0.1 AU), and by repeating the same argument as in Appendix E.2.1, we conclude that a binary system consisting of two 2-M_⊙ stars (or two 1-M_⊙ stars)—irrespective of the main-sequence/red-giant phase—can interact with the Galactic SMBH to produce an HVS with an ejection velocity of 500–600 km s⁻¹.

E.3. Ejection conditions of WINERED-HVS1 inferred from our simulations

Based on the simulations described above, we obtain the following insights into the ejection environment of WINERED-HVS1, assuming that it belonged to an equal-mass binary just before it was ejected from the SMBH.

- Judging from the ejection velocity of WINERED-HVS1 (500–600 km s⁻¹), we see that the binary separation a is ~ 0.5 –4 AU and the binary’s closest approach of the SMBH is $r_{\text{peri}} \sim 30$ –300 AU.
- When WINERED-HVS1 was ejected from the Galactic center, it could be a main-sequence star or a red giant.

¹⁹ The Roche radius of an equal-mass binary is given by $R_{\text{Roche}} = 0.38a$. By equating the Roche radius and the radius of a 3-M_⊙ main-sequence star (~ 0.011 AU), we obtain the minimum allowed value of a .

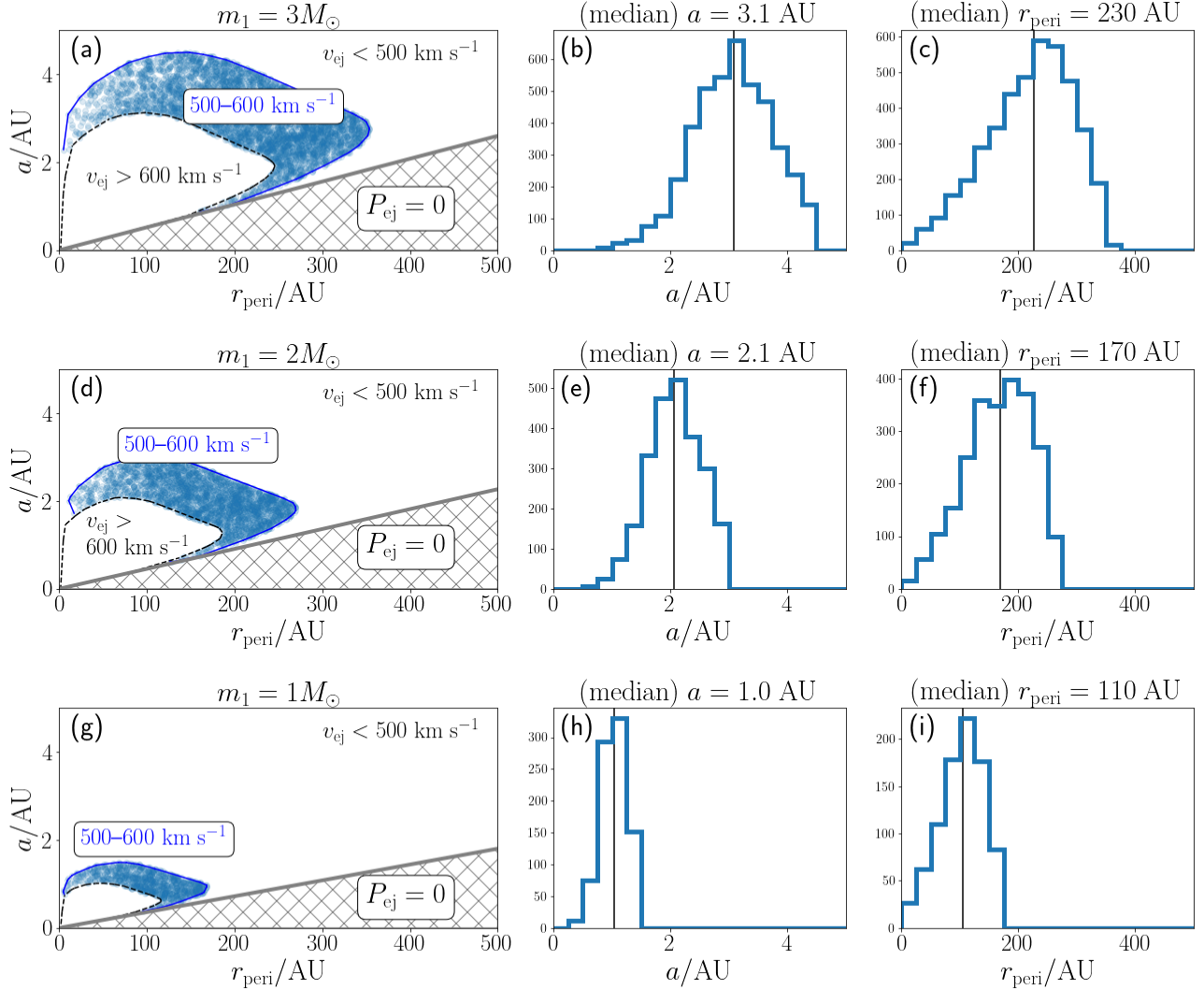


Figure 11. Results of Monte Carlo simulation of HVSs. On the top row (a–c), middle row (d–f), and bottom row (g–i), we show the results for simulated HVSs with masses of $3M_{\odot}$, $2M_{\odot}$, and $1M_{\odot}$, respectively. Panels (a), (d), and (g): The blue dots shows the distribution of (r_{peri}, a) that allows the ejection of an HVS to attain ejection velocity of $500\text{--}600 \text{ km s}^{-1}$. The hatched region corresponds to a parameter subspace where no ejection happens ($P_{\text{ej}} = 0$; $D > 175$). Panels (b), (e), and (h): The marginalized distribution of a for HVSs with $v_{\text{ej}} = 500\text{--}600 \text{ km s}^{-1}$. The vertical line shows the median of a . Panels (c), (f), and (i): The marginalized distribution of r_{peri} for HVSs with $v_{\text{ej}} = 500\text{--}600 \text{ km s}^{-1}$. The vertical line shows the median of r_{peri} .

- The timescales for 1-, 2-, and $3M_{\odot}$ stars to evolve from the main-sequence stage to the red giant stage (with a similar temperature to WINERED-HVS1) are roughly 20 Myr, 30 Myr, and 500 Myr, respectively. These timescales are longer than the time since the last disk crossing (14 Myr). Thus, if it was ejected from the Galactic center as a main-sequence star, it must have experienced one or more disk crossings after the ejection.
- If WINERED-HVS1 was recently ejected from the Galactic center and has never experienced disk crossings after the ejection, it must have been ejected as a red giant.

F. PROPERTIES OF OUR HVS CANDIDATE AND THE THEORETICAL PREDICTIONS

In this paper, we identify 22 HVS candidates, and one of the candidates, WINERED-HVS1, is a promising candidate in terms of its chemistry. Here we investigate whether our discovery of one HVS (candidate) is statistically natural.

F.1. Basic properties of WINERED-HVS1

First, we ignore the fact that this star is an HVS candidate and investigate the other observational properties (such as its magnitude) of WINERED-HVS1 from a statistical perspective. Based on the Gaia DR3 catalog, its G_{RP} , G , and G_{RVS} magnitudes are $G_{\text{RP}} = 13.58$, $G = 14.28$, and $G_{\text{RVS}} = 13.26$. Among 1.7 billion stars in the Gaia DR3, only 1% of them have G_{RP} or G values that are brighter than WINERED-HVS1. Also, among 219 million stars with Gaia XP spectra, only 9% of them have G_{RP} or G values that are brighter than WINERED-HVS1. These numbers indicate that WINERED-HVS1 is a bright object. However, except for its brightness, WINERED-HVS1 is not particularly special. By randomly selecting stars with similar G_{RP} magnitudes ($13.56 < G_{\text{RP}} < 13.60$), we find 91% of them have Gaia XP spectra, 88% have line-of-sight velocity (v_{los}) measurements by Gaia, 87% have good parallax measurements ($\text{parallax_over_error} > 5$), and 74% satisfy all the criteria above (as WINERED-HVS1 does). The fractions are almost identical if we select stars based on G -magnitude ($14.26 < G < 14.30$) instead.

F.2. Complications in the mock HVS catalog in Marchetti et al. (2018)

Marchetti et al. (2018) predicted the populations of HVSs observable in the Gaia catalog. Their HILLS mock catalog is a simulated catalog of both bound and unbound HVSs ejected from the Galactic center, assuming an HVS ejection rate of $2.8 \times 10^{-4} \text{ yr}^{-1}$. Since WINERED-HVS1 is identified as a bound HVS candidate, their HILLS catalog is appropriate for comparison with our results. However, before using their results, we must clarify three key differences between their identification of HVSs in the simulation and our search for HVS candidates.

(Complication 1):

We selected HVS candidates from a catalog of 48 million stars in Hattori (2025). In creating this catalog, Hattori (2025) did not use the full list of stars with Gaia XP spectra, which consists of 219 million stars. Instead, he focused on the 48 million stars located in regions with low dust extinction with $E(B - V) < 0.1$. Consequently, our search for HVSs is inevitably restricted to those HVSs in regions with low dust extinction. In contrast, Marchetti et al. (2018) used a 3D dust extinction map to generate dust-obscured photometric data for their simulated HVSs. Their synthetic data included HVSs from both high and low dust extinction regions. If we crudely assume that the spatial distribution of stars with Gaia XP spectra is similar to that of the HVSs,²⁰ we can estimate that we are searching for HVSs from approximately 22% of the available data (48 million/219 million).

(Complication 2):

Since Marchetti et al. (2018) only estimated the expected number of main-sequence HVSs, we need to be careful when using their mock catalog to assess the likelihood of discovering a red-giant HVS, such as WINERED-HVS1. The key differences between main-sequence HVSs and red-giant HVSs (with the same initial masses) are that the main-sequence phase lasts longer, and a red giant is intrinsically brighter.

According to the Padova isochrone model (Bressan et al. 2012), a $\sim 2M_{\odot}$ main-sequence star becomes approximately 1 mag brighter when it evolves into a red giant (except at the very final stage of the red giant phase when it becomes ~ 4 mag brighter). Additionally, the duration of the red-giant phase is only 21% of the main-sequence phase for a star with an initial mass of $2M_{\odot}$. An increase of brightness by 1 mag allows a magnitude-limited survey to cover 2.5 times larger distances and 16 ($= 2.5^3$) times larger volumes. Fig. 8 of Marchetti et al. (2018) predicted ~ 95 main-sequence HVSs with $G_{\text{RVS}} < 13.26$ (as bright as or brighter than WINERED-HVS1) and ~ 380 main-sequence HVSs with $G_{\text{RVS}} < 14.26$ (which extends the upper limit by 1 mag). Thus, in their analysis, increasing the G_{RVS} by 1 mag results in a 4 ($= 380/95$) times larger number of main-sequence HVSs. Based on these arguments, we expect that an increase of 1 mag in HVS brightness may lead to an increase in its detectability by a factor of 4 to 16. Considering the short duration of the red-giant phase, we estimate that the detectability of a $2M_{\odot}$ red-giant HVS may be around $f_{\text{RG/MS}} = 0.8\text{--}3.4$ ($= 0.21 \times (4\text{--}16)$) times that of a main-sequence HVS with the same mass. Similarly, the detectability of a $3M_{\odot}$ red-giant HVS is $f_{\text{RG/MS}} = 0.3$ ($= 0.15 \times (2.0\text{--}2.1)$) times that of a main-sequence HVS with the same mass; and the correction factor is $f_{\text{RG/MS}} = 0.2\text{--}0.8$ ($= 0.05 \times (4\text{--}16)$) for the case of $1M_{\odot}$ red-giant HVS. By combining these results, we infer that the detectability of a red-giant HVS with a mass of $1\text{--}3M_{\odot}$ may be around $f_{\text{RG/MS}} = 0.2\text{--}3.4$ times that of a main-sequence HVS with the same mass.

(Complication 3):

The simulated HVSs described in Marchetti et al. (2018) includes all the HVSs irrespective of the flight time, as long as the observational constraints (e.g., apparent magnitude) are satisfied. In contrast, in this paper, we aimed to identify HVSs by using the stellar orbits in the last 200 Myr. Our search is optimized for recently-ejected HVSs, and we may miss some fraction of HVSs ejected long time ago if their last disk crossings occurred at $R \gtrsim 200 \text{ pc}$.

²⁰ This approximation may not be as inaccurate as it seems. Most of the stars with Gaia XP spectra are disk stars and have a flattened distribution. The spatial distribution of HVSs in the left panel of Fig. 10 from Marchetti et al. (2018) also appears slightly oblate (even after accounting for the figure's aspect ratio). This flattened distribution may be due to bound HVSs being drawn toward the Galactic mid-plane because of the gravitational pull from the stellar disk.

In a pessimistic scenario, our search method may identify no HVSs that were ejected long time ago, and it may only identify recently-ejected HVSs. Based on our analysis in [Table 2](#), the typical flight time for recently ejected HVSs is approximately 20 Myr. Therefore, in this pessimistic scenario, we might have excluded HVSs with flight times longer than ~ 20 Myr. Suppose that WINERED-HVS1 is indeed a recently-ejected HVS (with no disk crossings after the ejection). Then, given the following points: (i) HVS ejections can occur at any time during a star’s lifetime, (ii) the estimated lifetime of WINERED-HVS1 is $\sim 0.5\text{--}10$ Gyr, and (iii) the typical flight time of recently ejected HVSs is ~ 20 Myr, it can be inferred that identifying one recently ejected HVS candidate (WINERED-HVS1) may suggest the existence of $\sim 25\text{--}500$ ($= 0.5\text{--}10$ Gyr/20 Myr) bound HVSs with similar characteristics to WINERED-HVS1 in our input catalog. In reality, we cannot determine whether WINERED-HVS1 was truly ejected recently; it may have been ejected in the more distant past. Thus, the correction factor ($\sim 25\text{--}500$) is an upper limit.

F.3. Assessment of the likelihood to find one red-giant HVS

Despite the complications mentioned above, we dare to explore how our discovery of one HVS (candidate) can be interpreted in the context of the theoretical predictions made by [Marchetti et al. \(2018\)](#). Since [Marchetti et al. \(2018\)](#) only considered main-sequence HVSs, we first pretend as if we found a ‘main-sequence’ HVS with $G_{\text{RVS}} = 13.26$.

As predicted in Fig. 8 of [Marchetti et al. \(2018\)](#), we assume that there are ~ 95 main-sequence HVSs with $G_{\text{RVS}} < 13.26$ (i.e., at least as bright as WINERED-HVS1). Also, we assume that 74% of Gaia stars with this same magnitude range possess Gaia XP spectra, v_{los} , and reliable parallax measurements (see [Section F.1](#)), and that 22% of HVSs are found in low dust extinction regions (see (Complication 1)). Then we expect to identify ~ 15 ($= 95 \times 0.74 \times 0.22$) main-sequence HVSs that meet the following criteria: (i) $G_{\text{RVS}} < 13.26$, (ii) located in low dust extinction regions ($E(B - V) < 0.1$), and (iii) possessing the Gaia XP spectra, velocity measurements, and reliable parallax.

As noted in (Complication 2), what we found is a red-giant HVS candidate with a mass of $1\text{--}3M_{\odot}$ (WINERED-HVS1), which is more likely to be detected by a factor of 0.2–3.4 than a main-sequence HVS with the same mass. After correcting for this factor, the expected number of red-giant HVSs is 3–51 ($= 15 \times (0.2\text{--}3.4)$). Although this number is associated with a large uncertainty, finding one HVS candidate from our input catalog is less than this theoretical prediction. In this regard, it is worthwhile mentioning that this prediction includes all the observable HVSs irrespective of the flight time. For example, as discussed in (Complication 3), recently ejected HVSs might represent $\sim 1/500\text{--}1/25$ of the entire HVS population with similar properties. In this regard, the theoretical prediction for the recently ejected HVSs is 0.006–2. (Here, we adopt $3/500 = 0.006$ as the lower limit and $51/25 \simeq 2$ as the upper limit.) If we assume that WINERED-HVS1 is truly a recently ejected HVS, this theoretical prediction may be consistent with our discovery of one HVS candidate. However, we need to stress that, even if WINERED-HVS1 is a genuine HVS ejected from the Galactic center, we currently do not have a way to rigorously constrain the flight time of this star.

Also, Fig. 11 (top panel) and Fig. 7 of [Marchetti et al. \(2018\)](#) indicate that the majority of HVSs with $G_{\text{RVS}} < 16$ have total velocities of $v < 500 \text{ km s}^{-1}$ and are located at the Galactocentric distances of $r < 10$ kpc. These findings are consistent with WINERED-HVS1, which has a velocity of $v = 273 \text{ km s}^{-1}$ and is located at $r = 5.45$ kpc. These characteristics suggest that the HVS candidate we identified may represent a typical bound HVS in the Gaia data.

G. ORBITAL PROPERTIES OF METAL-RICH HVS CANDIDATES

In [Fig. 5](#), we show the properties of WINERED-HVS1. Here we show the orbital properties for mrHVSsp1-9 in [Figs. 12](#) and [13](#). We show the plots for mrHVSxp2-13 in [Figs. 14](#), [15](#), and [16](#).

H. NOTATIONS IN THIS PAPER

[Table 6](#) summarizes the notations for astrometric quantities and chemical abundances used in this paper.

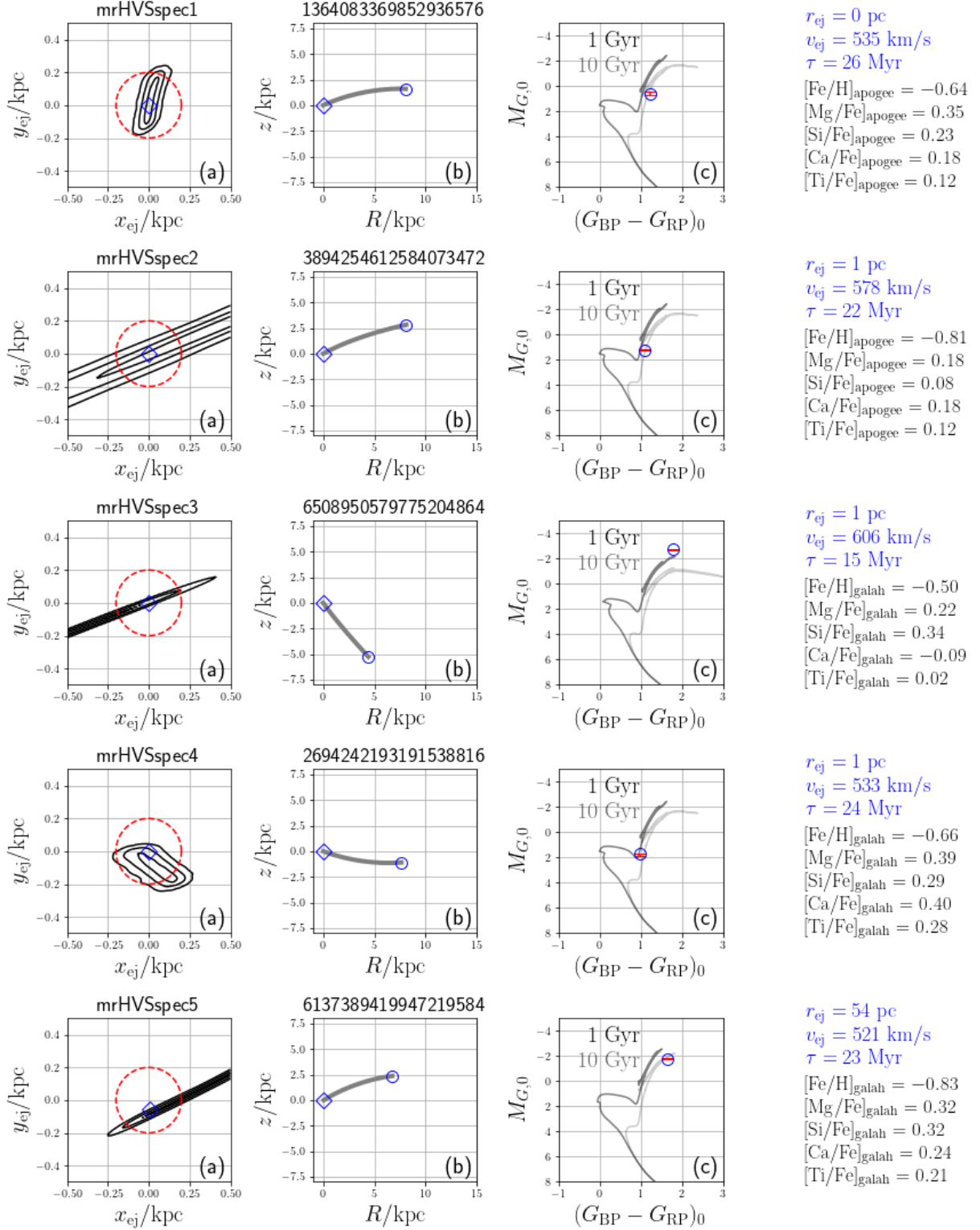


Figure 12. The same as Fig. 5 but for mrHVSspec1-5.

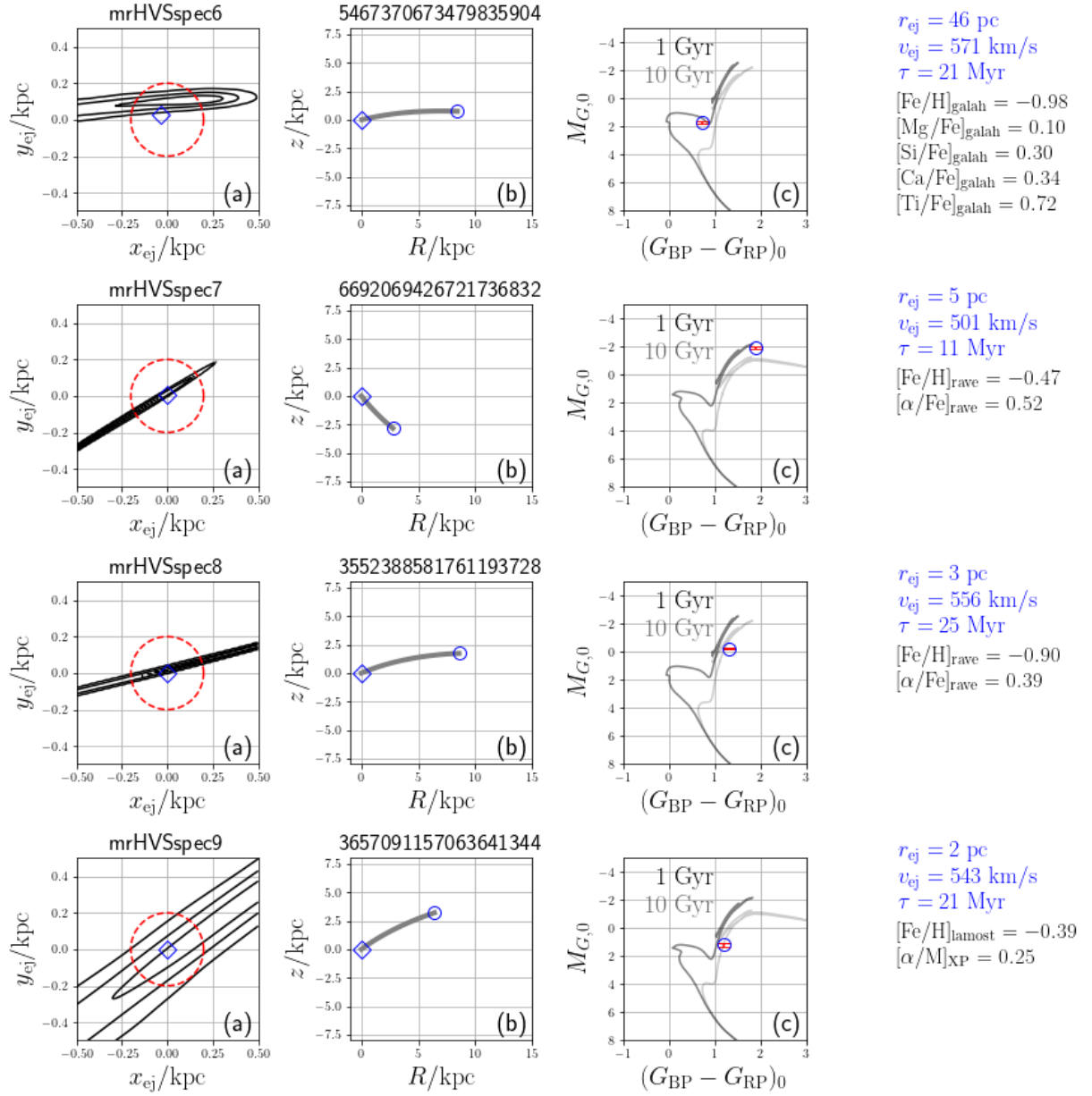


Figure 13. The same as Fig. 5 but for mrHVSspec6-9.

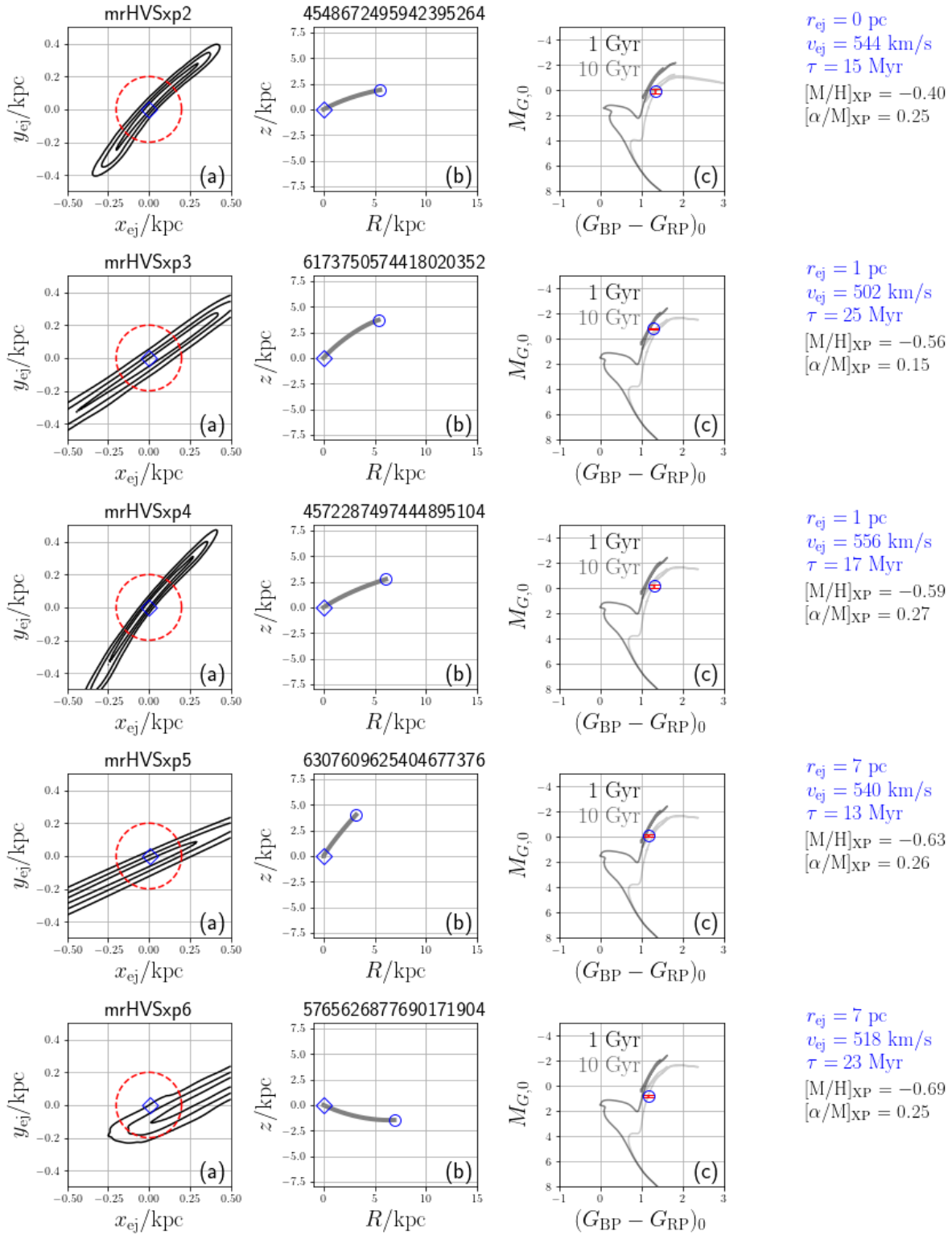


Figure 14. The same as Fig. 5 but for mrHVSxp2-6.

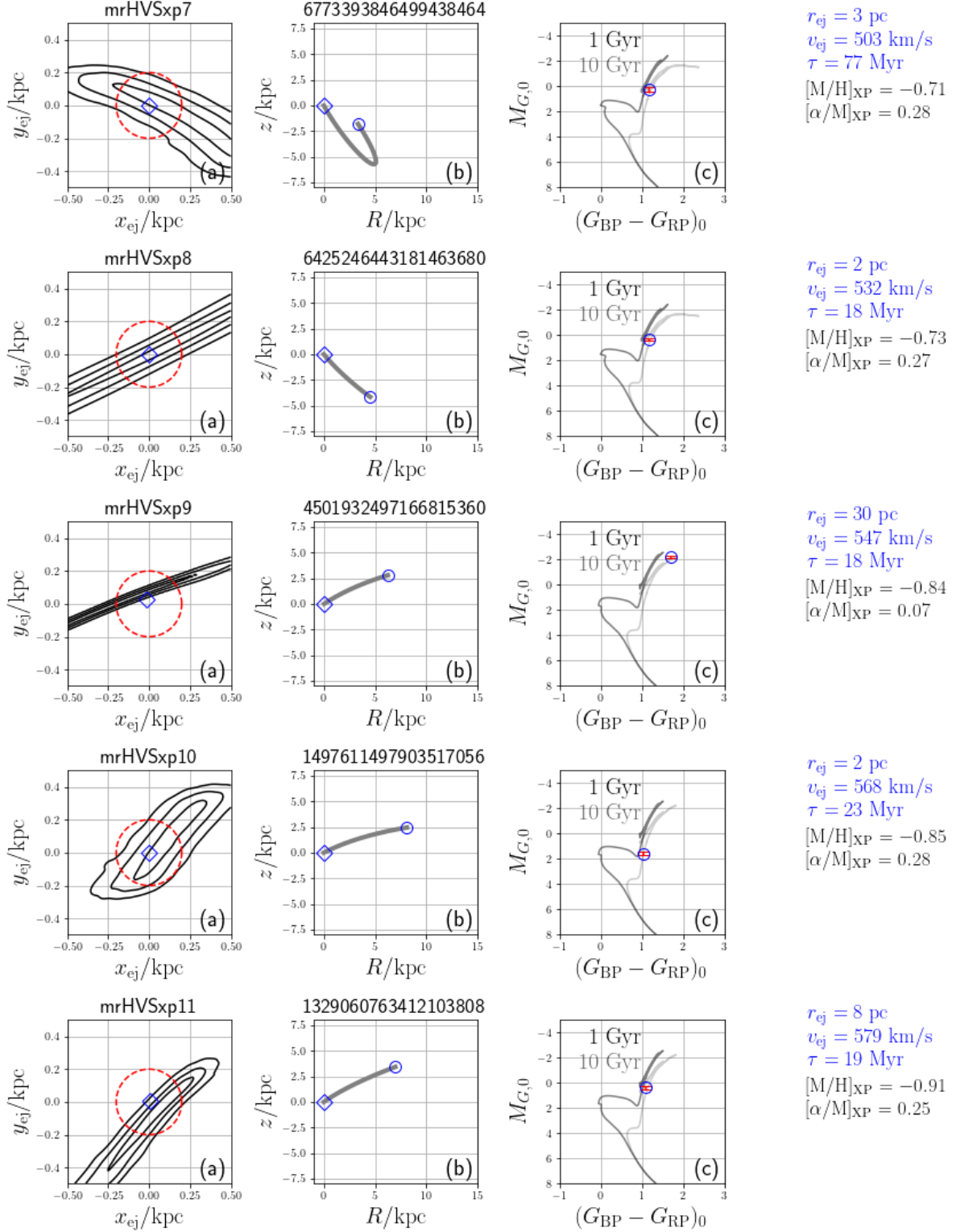


Figure 15. The same as Fig. 5 but for mrHVSxp7-11.

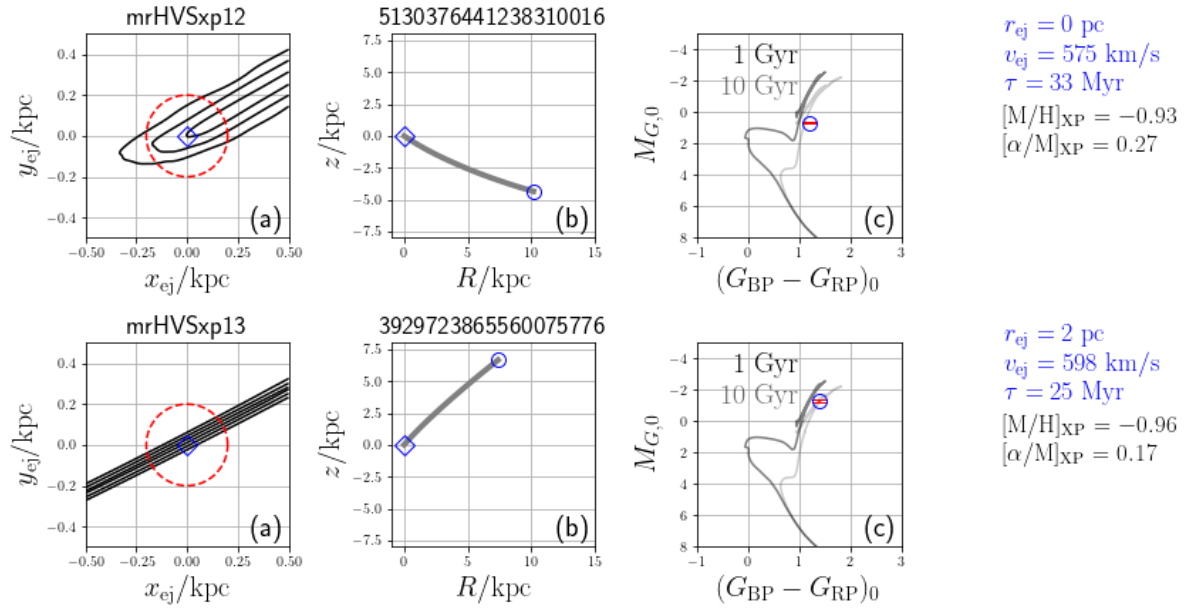


Figure 16. The same as Fig. 5 but for mrHVSxp12-13.

Table 6. Notations in this paper

Quantity	Meaning
α	Right ascension
δ	Declination
d	Heliocentric distance
ϖ	Parallax
σ_{ϖ}	Parallax error
$\mu_{\alpha*}$	Proper motion in α
μ_{δ}	Proper motion in δ
v_{los}	Heliocentric line-of-sight velocity
$[M/H]_{\text{XP}}$	Metallicity $[M/H]$ determined from Gaia XP spectra (Hattori 2025)
$[\alpha/M]_{\text{XP}}$	α -abundance $[\alpha/M]$ determined from Gaia XP spectra (Hattori 2025)
$[X/Y]_{\text{spec}}$	Spectroscopically determined chemical abundance $[X/Y]$
$[\alpha/Fe]_{\text{spec}}$	Spectroscopically determined α -abundance. ^(a)

NOTE— (a) If $[\alpha/Fe]_{\text{spec}}$ is in the literature, we use the literature value. If not, we compute $[\alpha/Fe]_{\text{spec}}$ from available abundance ratios of α elements. If four abundance ratios $[Mg/Fe]$, $[Si/Fe]$, $[Ca/Fe]$, and $[Ti/Fe]$ are available, we compute the average and standard deviation of these four values and use them as $[\alpha/Fe]_{\text{spec}}$ and the associated uncertainty. (In computing these average, we ignore the uncertainties in each abundance ratios.) If only some of the four ratios are available, we take the average and standard deviation of the available ratios.